NTNU

Norwegian University of
Science and Technology

Evaluation of a Capacitive Micromachined Ultrasonic Transducer with backing layer

Per-Martin Ødelund

Master of Science in Electronics
Submission date: August 2010
Supervisor: Arne Rønnekleiv, IET
Co-supervisor: Sigrid Berg, IET

Norwegian University of Science and Technology
Department of Electronics and Telecommunications

Problem Description

A research project at the Department of Electronics and Telecommunication at NTNU is developing technologies for intravascular ultrasound imaging to simplify detection and characterization of atherosclerotic plaque. The Capacitive Micromachined Ultrasonic Transducer (CMUT) array has been chosen due to good matching with fluids as measuring media and good bandwidth, giving it the needed properties to detect and characterize atherosclerotic plaque.

The student is tasked with performing measurements to characterize the behavior of a CMUT with a backing layer. This is the same CMUT as the one tested in the project Characterization of Capacitive Micromachined Ultrasonic Transducers, and this will be a continuation of the evaluation of said CMUT. An assessment of the performance of the backing layer, and the effect it has on the CMUT should be made, in addition to an evaluation of the CMUTs general performance.
The student should also show awareness of the measuring method and equipment, and any effect or limitation they add to the result.

Assignment given: 13. April 2010
Supervisor: Arne Rønnekleiv, IET

Abstract

One of the leading causes of death in the western world today is heart diseases, and atherosclerotic plaque that ruptures in the coronary arteries is believed to be one of the main causes of heart attacks. The Capacitive Micromachined Ultrasonic Transducer has good acoustic matching with fluids, and is considered a good candidate for improving intravascular ultrasound diagnostics.

Further evaluation and characterization of a CMUT operating in immersion has been the objective of this thesis, and it is a continuation of the work started in the project *Characterization of Capacitive Ultrasonic Transducers*. The same CMUT have been studied in both, but a backing layer was added to it for the testing done during the work on this thesis.

Pulse-echo measurements with the CMUT immersed in rapeseed oil have been performed, and there has also been conducted measurements to find the attenuation of the oil. The results from the attenuation measurements have then been employed to simplify the analysis of the pulse-echo measurements.

Any definitive characteristics for the CMUT was not found during these tests due to disturbances in the frequency responses. This is suspected to be because of line resistances and parasitic capacitances in the system. This suspicion is supported by the findings from studying the impedance response of the system.

The backing layer added to the CMUT have proved to be very effective in dampening the ringing effect on the pulses emitted by the CMUT. There have also been signs of unexpected alteration of the CMUTs frequency characteristics. One possible source of this is that the process of adding the backing layer have resulted in that the layer exerts force on the CMUT, and by this changing the tension of the membranes.

Preface

This thesis presents the work conducted during the last semester of my masters degree at the Department of Electronics and Telecommunications of the Norwegian University of Science and Technology (NTNU). This has been a continuation of the work started in my project from the autumn of 2009, in connection to the *SMiDA* group project.

I would like to thank my supervisors Professor Arne Rønnekleiv and Ph.D. candidate Sigrid Berg at the Department of Electronics and Telecommunications for their guidance and understanding. I thank Ph.D. candidate Kamal Raj Chapagain for providing and helping me with the backing layer to the CMUT.

Tore Landsem and the rest of the machine shop should also be mentioned for helping out with the test equipment, and lending me tools for setup adjustments. I would also like to extend my gratitude to Tor-Arne Ødelund, Kristine Welde and Jarle Larsen, for giving feedback on my writing.

Per-Martin Ødelund
NTNU, Trondheim
August, 2010

Contents

1. Introduction

Cardiovascular diseases are one of the leading causes of death today in developed countries[1]. The main cause of heart attacks is atherosclerotic plaque in the coronary arteries[2]. The plaque is a build up of fatty lipids inside the artery walls, where only a thin part of the wall separates it from the blood stream. If the artery wall is ruptured, the lipids can be released into the bloodstream and cause the formation of blood clots big enough to block the artery. This chokes off the oxygen supply to the heart muscles and can initiate a heart attack(coronary thrombosis), and thus cause permanent damage to the heart muscle.

Detection of plaque in the coronary arteries can be difficult with today's equipment and methods. An angiogram is a detailed picture of a blood vessel, and this is usually obtained by injecting a dye into the vessel that is detectable with x-rays[3]. This method has a drawback since it only gives a view of the areas where the blood flows, and even if it shows where there is stenosis(narrowing) of the opening in the artery it does not present the reason and extent of the problem[4][5].

A research project called *Smart Microsystems in Diagnostic Imaging in Medicine (SMiDA)* at the Department of Electronics and Telecommunication at the Norwegian University of Science and Technology(NTNU), has been developing technologies for intravascular ultrasonic imaging. The goal of this project is to make detection of atherosclerotic plaque easier[6]. The *Capacitive Micromachined Ultrasonic Transducer* (CMUT)array, with its good matching with fluids as measuring media and wide bandwidth, has the needed properties to detect and characterize atherosclerotic plaque[7]. It was therefore chosen as the transducer technology to use in the SMiDA project[6].

The work done in *Characterization of Capacitive Micromachined Ultrasonic Transducers*[8] consisted of construction of a test rig, initial behaviour tests, and pulse-echo characterization measurements on a CMUT immersed in rapeseed oil. The result of these measurements were inconclusive. This was because of an irregular behaviour in the frequency response, believed to be arising from phase shifts in the CMUT array due to line resistances and capacitances.

The objective of this thesis is to produce a more thorough evaluation of the CMUT by continuing and expanding the work started in [8]. To accomplish this, a set of pulse-echo immersion measurements will be performed on the same CMUT, but with an addition of a backing layer on the backside of the CMUT chip.
The purpose of this layer is to reduce what is called ringing, which is self induced resonant waves in the CMUT chip that extends the emitted pulse duration [9]. By dampening the ringing, a more stable response may be produced by the CMUT, and this will hopefully be easier to evaluate.

In an effort to reduce the number of variables to account for in the analysis of the results, the attenuation of the rapeseed oil will be measured so that it can be compensated for. A separate test system to measure the attenuation will be set up to achieve this.

Measurements of the system impedance response will also be carried out, in order to get an impression of the systems electrical properties.

2. Background

Ultrasound transducers have traditionally used piezoelectric crystals for exciting and detecting ultrasonic waves. Piezoelectric materials change dimensions due to applied electric fields [10], and create electric fields when subjected to external force. This is utilized to emit and receive ultrasonic waves. There are however several drawbacks with these transducers where the measurements are gas or fluid coupled[11], with the most significant one being impedance mismatch between the piezoelectric material and the medium. For air the magnitude of mismatch is in the order of 10^6, and 30 for water. This mismatch means that it will not be possible to achieve good efficiency with this type of transducer in these media without adding means to increase the matching. This problem is usually solved by attaching a matching layer between the piezoelectric material and the medium. This layer has a characteristic impedance to compensate for the mismatch, but this comes with the price of restrictions in design and narrower bandwidth [11].

Another approach for generating sound waves in general is to make a membrane vibrate. The ongoing development of integrated circuit fabrication technology to achieve greater downscaling have also contributed to the development of micromachining technology for fabrication of microelectromechanical systems (MEMS). This has given the opportunity to fabricate silicon devices operating at ultrasonic frequencies. The CMUT is such a device and it is in terms of efficiency and bandwidth comparable to its piezoelectric counterpart [12], and can be designed to overcome the drawbacks presented for the piezoelectric transducer. The CMUT also has an advantage of having access to the tools of IC fabrication making fabrication of CMUTs with a wide range of shapes and sizes on both membranes and arrays available. This opens up for precise control of resonance frequency and bandwidth [13] to make it fit the medium and measuring task.

2.1 Ultrasonic waves

2.1.1 Wave propagation mechanism and properties

By exerting force on a system of mass particles, e.g a fluid, the particles can be shifted from their equilibrium state causing a disturbance in the fluid. If this force is applied repeatedly, an oscillatory motion of the particles will occur, and a wave will propagate in the fluid due to the bonds between neighboring particles. This wave can be characterized by a set of properties as follows:

- Wavelength, λ.
- Oscillation period, T.
- Frequency, f.
- Propagation velocity, c.
- Displacement amplitude, A_0.

Equations (2.1) and (2.2) state relations between these properties.

$$f = \frac{1}{T}. \tag{2.1}$$

$$\lambda = cT = \frac{c}{f}. \tag{2.2}$$

Waves with frequencies higher than 20kHz, which is the highest frequency the human ear can detect, are defined as ultrasonic waves[14].

2.1.2 Reflection, transmission and refraction

Ultrasonic wave propagation will be affected by boundary surfaces encountered. At these boundaries, reflection will occur and for a slanted boundary there will be refraction. For large enough boundary surfaces the laws of reflection and refraction known from geometrical optics can be applied to the incident ultrasonic beam[15][14][16]. An ultrasonic wave with perpendicular incidence to a boundary between medium A and B is shown in Fig 2.1.

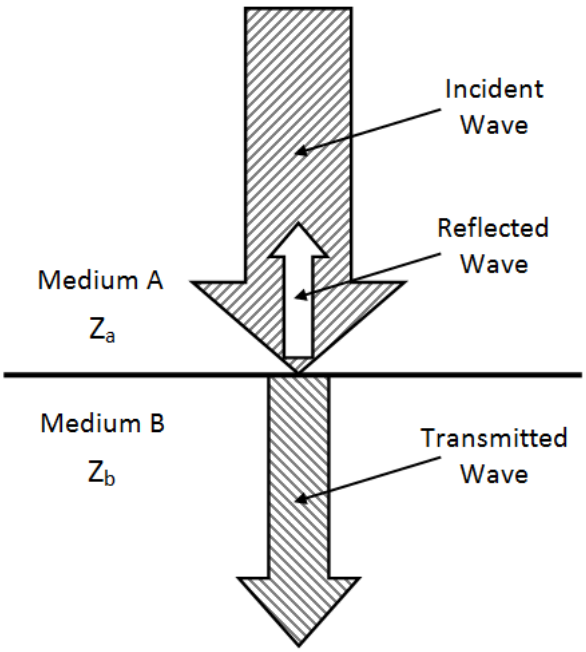

Figure 2.1: Ultrasonic wave with perpendicular incidence on a boundary.

Medium A and B has an acoustic impedance Z_a and Z_b respectively, and the wave has an initial intensity of I_{a1}. After hitting the boundary, a reflected wave with intensity I_{a2} propagates back in medium A, while a wave of intensity I_{b1} have penetrated into medium B.
The ratio between the reflected and incident wave is called the reflection coefficient (R_0), and is in [15] stated and extended in equation (2.3) as

$$R_0 = \frac{I_{a2}}{I_{a1}} = \left(\frac{Z_b - Z_a}{Z_b + Z_a}\right)^2 \leq 1. \tag{2.3}$$

A similar relation exists for the case of a transmission line. This is presented in Section 2.9. Since the relation between the intensities of the incident, reflected and transmitted waves are given as

$$I_{b1} = I_{a1} - I_{a2}, \tag{2.4}$$

the transmission coefficient (D) can be given by R_0 as shown in equation (2.5).

$$D = \frac{I_{b1}}{I_{a1}} = \frac{I_{a1} - I_{a2}}{I_{a1}} = 1 - R_0 \leq 1. \tag{2.5}$$

For situations where the incident wave hits the boundary at an angle, Snell's law of refraction can be applied. This law describes the behaviour of the reflected wave and refraction of the wave transmitted into the second medium. Snell's law is stated as

$$\frac{\sin\theta}{\sin\phi} = \frac{c_a}{c_b}, \tag{2.6}$$

where θ is the angle of incidence, and ϕ is the angle of refraction. The variables c_a and c_b are the propagation velocities of sound in medium A and B respectively, and this relation is therefore independent of the acoustic impedance of the media. A graphical description of the effects Snell's law describes can be seen in Fig 2.2.

2.1.3 Ultrasonic near and far fields

An ultrasound source of comparable dimensions to the emitted wavelength will emit spherical wavefronts which diverges rapidly. A source with larger dimensions than the wavelength of the sound produced can be considered as many individual sound sources, producing their own spherical wavefronts[17]. These wavefronts will in accordance with Huygens' principle interact with each other and produce intensity variations in the propagation direction due to constructive and destructive interference.

This results in a complex wave pattern in front of the source in what is called the *near field*. A key property of this field is that the ultrasound beam does not diverge, but maintains its width. After a certain distance the alternating intensity of the near field ends with a maximum that slowly decreases, and this is the beginning of the *far field*[18]. Fig 2.3 shows a sketch of the variation of the intensity as a function of distance from the source.

The distinctive properties of the far field are the uniform intensity and divergence[17]. Divergence is a source of loss as it spreads the energy continuously over the distance traveled, and the received signal will then be weaker. The spread also results in a decrease in lateral resolution.

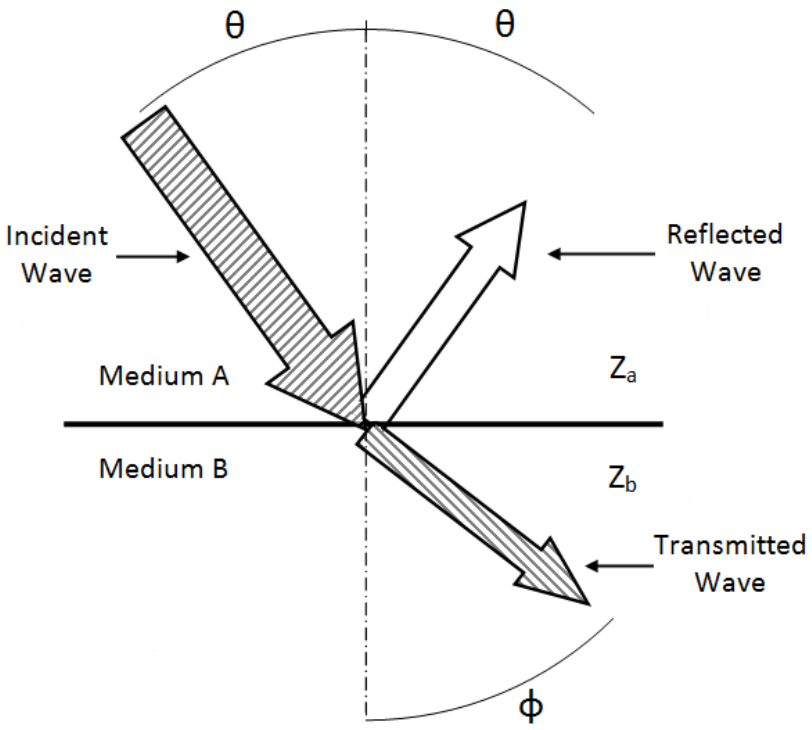

Figure 2.2: Ultrasonic wave reflection and refraction when incident wave has an angle α onto the boundary.

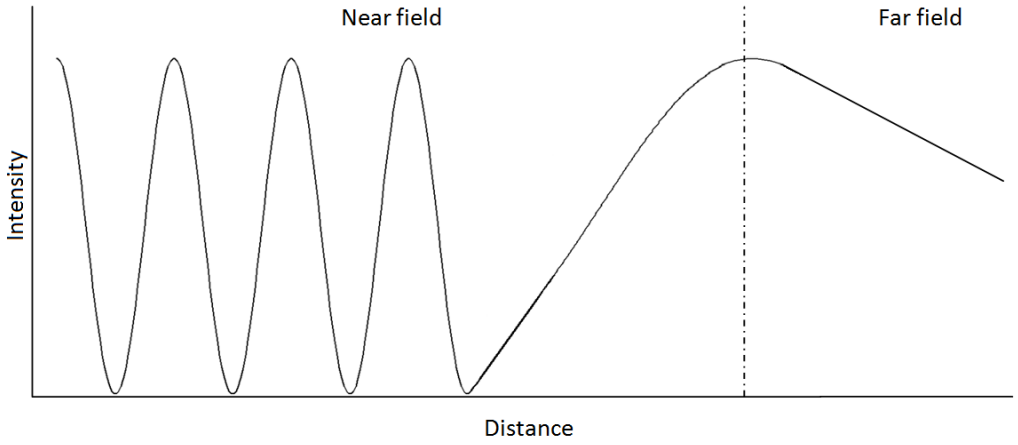

Figure 2.3: A sketch of the intensity as a function of distance from the source.

A common formula for the near field depth (NFD) for a circular source exists, and is given in [17] as

$$NFD = \frac{D^2 f}{4c} = \frac{D^2}{4\lambda} = \frac{r^2}{\lambda}, \tag{2.7}$$

where D is the diameter, and r is the radius of the source.

This formula is sometimes extended to fit a rectangular area, but according to [18] it is not sufficiently accurate. The same article presents however a relation for where the far field starts for a rectangular source. This is

$$FF > \frac{b^2}{2.88\lambda}, \tag{2.8}$$

where b is the longest side of the rectangular area.

2.2 CMUT structural description

The CMUT is essentially a parallel plate capacitor where one of the electrodes is suspended on a thin membrane over a small gap. The CMUT is fabricated on a p-doped substrate which will act as the anchored electrode. The membrane and cavity support structure is formed by an insulating material where silicon nitride (Si_3N_4) is the most common choice [12]. A metal layer is deposited on top of the membrane to form the suspended electrode. A simple cross sectional schematic of a basic CMUT structure and signal connections is shown in Fig 2.4.

In order to avoid problems with mechanical loading due to cushioning effects on the backside of the membrane, the cavity can be evacuated and sealed. This also serves to keep contaminants out so that the CMUT does not change its behavior over time, and it is essential for operation in immersion.

2.3 Operating principal of a CMUT

The CMUT can be used both for emitting and receiving ultrasound. This is done by either driving the membrane vibration by an AC signal for emission, or receiving by measuring the variation in deflection when pressure variations is induced on the membrane by the medium. Common for both modes is that it needs to have a bias voltage in order to work properly.

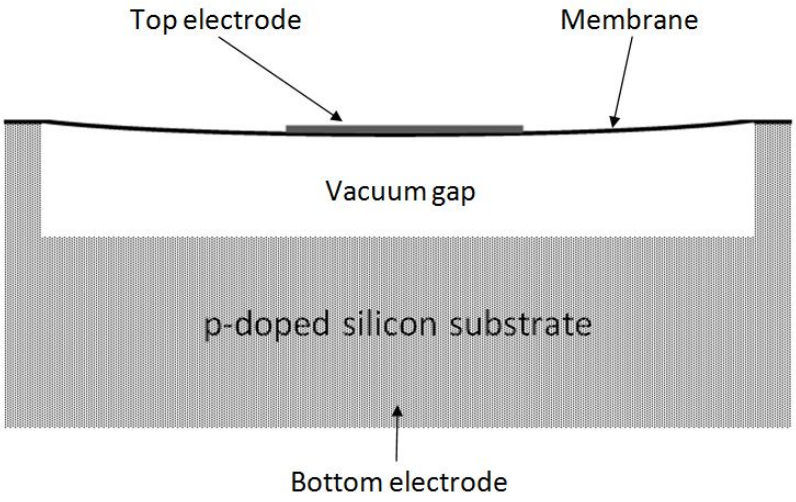

Figure 2.4: A cross sectional schematic of a CMUT (Not to scale).

Due to the unipolar nature of electrostatic attraction a qualitatively assessment would suggest that unless the CMUT is biased, the membrane would vibrate at double frequency compared to the driving signal. This is also shown through equations (2.9)-(2.16) by looking at the CMUT as a parallel plate capacitor where the suspended electrode can move without being deformed. Another assumption that will be made for these equations is that electric fringe fields can be ignored.

From [10] it is given that the value of the capacitance C between two plates is defined as

$$C \equiv \frac{Q}{V}, \tag{2.9}$$

where Q is the charge stored, and V is the potential over the plates. The stored energy U by the capacitor can be expressed as

$$U = \frac{1}{2}CV^2. \tag{2.10}$$

The electric field E is according to Gauss' law related to Q by

$$E = \frac{Q}{\epsilon A}, \tag{2.11}$$

where ϵ is the permittivity of the media between the electrodes, and A is the area of the plate. It is also related to V by

$$V = E \cdot d, \tag{2.12}$$

where the variable d is the distance between the plates. Using the relations (2.11) and (2.12) in equation (2.9) we get

$$C = \frac{Q}{E \cdot d} = \frac{Q}{\frac{Q}{\epsilon A} \cdot d} = \frac{\epsilon A}{d}. \tag{2.13}$$

With the electrostatic force being unipolar, the magnitude of the force between the plates in the capacitor is equal to the absolute gradient of U with respect to the variable d. Using the relations (2.10) and (2.12) this results in

$$F_{electric} = \left|\frac{\partial U}{\partial d}\right| = \frac{1}{2}\left|\frac{\partial C}{\partial d}\right| V^2 = \frac{1}{2}\frac{\epsilon A}{d^2}V^2 = \frac{1}{2}\epsilon A E^2. \tag{2.14}$$

The force is shown to be proportional to E^2, and by taking into account that the electric field has two contributors, E_{DC} and E_{AC}, an expression for E can be written

$$E = E_{DC} + E_{AC} = E_{DC} + E_{sig}\cos\omega t, \tag{2.15}$$

$$\begin{aligned} E^2 &= (E_{DC} + E_{sig}\cos(\omega t))^2 \\ &= E_{DC}^2 + 2E_{DC}E_{sig}\cos(\omega t) + E_{sig}^2\cos^2(\omega t). \end{aligned} \tag{2.16}$$

Setting the DC component in (2.16) to zero results in a vibration frequency twice as high as the driving signal. Biasing is therefore needed, and it also shows that E_{DC} needs to be larger than E_{sig} for the device to operate in a linear regime where it can be analyzed without having a complete understanding of its behaviour[11].

When the CMUT is used for receiving acoustic waves, the vibrations in the membrane are detected by measuring the variation in capacitance. A constant bias voltage is needed so that this variation in capacitance induces a current that the receiving circuitry can read.

2.4 Pull-in and collapse voltage

2.4.1 Pull-in

An important condition of parallel plate actuators or similar ones like the CMUT that should be kept in mind is *pull-in*. Pull-in occurs if the voltage over the device is increased to a point where the electrostatic forces pulling the electrodes together overcome the mechanical restoring force of the structure that suspends the moving electrode. This voltage is called the *collapse* or *pull-in voltage*. When this condition occurs, the moving electrode or the membrane and the top electrode in the CMUTs case is pulled down to the bottom of the gap as shown in Fig 2.5. It will stay there until the voltage is reduced to a lower level than the *snap-back voltage* of the device, as reported in [11].

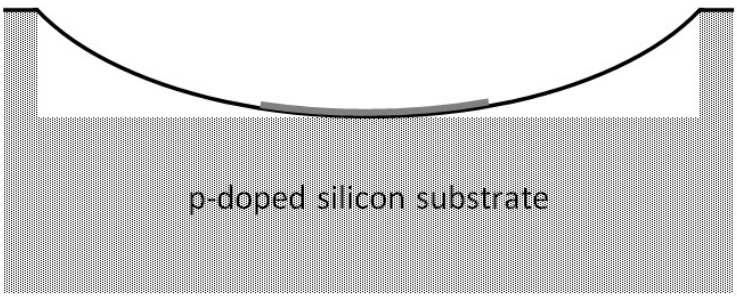

Figure 2.5: A cross sectional view of a collapsed CMUT (Not to scale).

While in pull-in the CMUT does not necessarily break down, but can continue to function as a vibrating ring, since the center of the membrane is pulled down to the bottom of the gap. Operation in this mode is reported in [19] to give a high coupling efficiency, and by that emit higher acoustic power compared to the traditional mode. However, for a CMUT designed to operate in the traditional mode, pull-in has to be avoided for the device to work.

2.4.2 Collapse voltage

For the membrane to be in equilibrium, the magnitude of the electrostatic force must be equal to the mechanical restoring force exerted by the inherent stress in the membrane. By assuming that the mechanical restoring force exerted by the inherent stress in the membrane is linear, this force can be expressed as

$$F_{mechanical} = kx, \tag{2.17}$$

where k is the mechanical spring constant and x is the displacement. The electrostatic force (2.14) can be rewritten as

$$F_{electric} = \left|\frac{\partial U}{\partial d}\right| = \frac{1}{2}\left|\frac{\partial C}{\partial d}\right| V^2 = \frac{1}{2}\frac{\epsilon A}{(d_0 - x)^2}V^2, \tag{2.18}$$

where d_0 is the initial position of the membrane at zero bias and pressure.

By evaluating these equations graphically one can see from Fig 2.6 that there are two points of intersection where $F_{electric}$ equals $F_{mechanical}$ at a given bias voltage. The system will be unstable at the one with the greatest displacement and will seek to settle at the other. The bias voltage that results in only one intersection is the collapse voltage, as any increase from this will cause the membrane to get pulled in. This is because there will be no intersection indicating that the restoring force cannot keep up with the electrostatic attraction.

An expression for the corresponding bias voltage for a given displacement can be written as:

$$V_{bias} = \sqrt{\frac{2kx}{A\epsilon}}(d_0 - x). \tag{2.19}$$

From [10] it is given that solving this for the case of the single intersection point gives the expression

$$x = \frac{d_0}{3}, \tag{2.20}$$

for the collapse point, which in turn results in

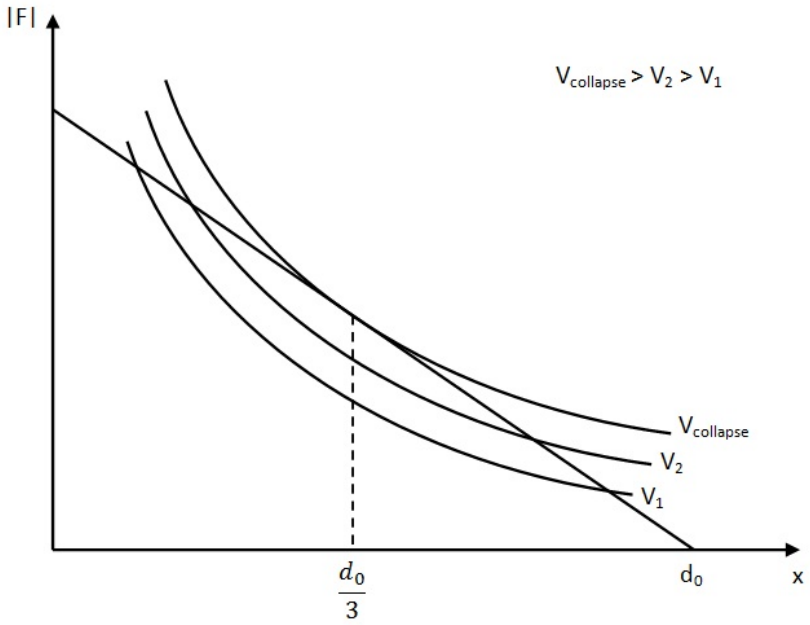

Figure 2.6: Magnitude of electrostatic attraction and mechanical restoring force versus membrane displacement.

$$V_{collapse} = \sqrt{\frac{8kd_0^3}{27A\epsilon}}, \tag{2.21}$$

for the collapse voltage.

2.5 Electromechanical coupling

The function of an acoustic transducer is to convert energy between the electrical and the mechanical energy domain. The electromechanical coupling coefficient is a fraction that says how much of the energy that is converted from one domain to another, and by this gives an impression of how effective the transducer is. In [12] it is stated that the coupling coefficient of a CMUT can be related to the displacement as

$$k_T^2 = \frac{2x}{d_{eff} - x}, \tag{2.22}$$

where d_{eff} is the effective gap height between the electrodes with the

membrane being an insulator at zero bias and pressure. If the displacement of the membrane is at the collapse point (2.20) $(d_0 = d_{eff})$, the coupling coefficient will approach unity which implies that all of the energy is converted from one domain to the other. This means that CMUTs operating in the non collapsed mode should be biased as close to the collapse voltage as possible to maximize efficiency.

2.6 Frequency and bandwidth

For a resonating structure like the CMUT, its behaviour depends on its structural dimensions and the medium it is operating in. In general, a resonant structure will have an increased resonant frequency with decreased dimensions, and the development of micromachining technology has made silicon structures resonating at ultrasonic frequencies possible.

Equation (2.23) is a formula for resonant frequency of a circular membrane of uniform thickness t, and shows the relation between the resonant frequency and membrane radius r [10].

$$f_{res} = \frac{k_{mem}}{2\pi}\sqrt{\frac{(\frac{Et^3}{12(1-\gamma^2)})g}{wr^4}}, \tag{2.23}$$

where k_{mem} is the membrane spring constant, g is the gravitational constant, w is the load, E is Young's modulus and γ is the shear strain.

The system can be looked at as a spring system where the electrostatic attraction drives the system, the membrane acts as the spring, and the surrounding medium will cause dampening. If surrounded by a medium of low mechanical impedance like air for instance, the impedance of the membrane itself will dominate, and a frequency response with a narrow peak around the center frequency is produced [10]. If however the surrounding medium is a fluid, its impedance is much greater and will cause dampening of the system. This shifts the center frequency to a lower one and gives a broadbanded frequency response around it.

For the CMUT it is preferred to have a high center frequency since high frequency gives better resolution, and broad bandwidth means a high temporal resolution which makes detection of defects that are close together possible[7]. One drawback with high frequencies is that ultrasound attenuation generally increases for increasing frequencies (See Section 2.7.1).

This results in reduced penetration depth for the transducer.

2.7 Attenuation and transmission losses

For an ultrasonic wave traveling through a material, the energy of the wave will bleed off as the wave propagates, i.e its amplitude will decrease. The main reasons for this are absorption and scattering[20] which adds up over the distance traveled. Other transmission losses like reflection and refraction of the wave[15] also occur.

2.7.1 Attenuation in fluids

Absorption in fluids occurs as a result of the viscosity of the fluid, which is a measure of the fluids resistance to shear and tensile stresses. This resistance causes a conversion of ultrasonic energy into other forms, and will eventually dissipate it as heat[14] [20].
The factor denoting the grade of attenuation is called the attenuation coefficient (α), and it can for fluids, as stated in [15] and [14], be expressed as

$$\alpha = \left(\frac{8\pi^2\eta}{3\rho c^3}\right) f^2 = \alpha_0 f^2. \tag{2.24}$$

In expression (2.24), η denotes dynamic viscosity, ρ is the density, and c is the speed of sound in the fluid. It should be noted that the expression in [14] is off by a factor of two, and has been corrected for use in this thesis.

This expression only considers dynamic/shear viscosity. This has however been shown to give considerably smaller values compared to attenuation measurements. An additional viscosity factor called *volume* or *bulk* viscosity need to be added to the expression to make it more accurate, and the expression becomes

$$\alpha = \frac{2\pi^2}{\rho c^3}\left(\frac{4\eta}{3} + \eta^v\right) f^2, \tag{2.25}$$

where η^v is the volume viscosity. The main points to note about these expressions are the relation $\alpha \propto f^2$, which means that attenuation increases

quadratically for increasing frequencies, and the relation to temperature due to the temperature dependencies of η and ρ.
The volume viscosity is related to a lag in flow of the fluid when experiencing acoustic pressure. This lag causes attenuation because the fluid can not keep up with the compression/expansion rate demanded at higher frequencies.

Scattering also contributes to the attenuation, especially in heterogeneous media where there are many particles that can interact with the wave. The size and concentration of these particles will affect the degree of attenuation contributed by scattering[15].

Note: Equations (2.24) and (2.25) produce values given in Neper per meter (Np/m). Neper is an equivalent of dB using the natural number instead of 10 as the logarithmic base. Converting to dB is done as follows:

$$1Np = \frac{20}{\ln 10} dB. \tag{2.26}$$

2.7.2 Transmission losses

In addition to attenuation, transmission losses due to reflection/ transmission and refraction can also add to the total loss of energy for a received wave. When a wave encounters a boundary between two media, a part of it will be reflected and the rest is transmitted into the second medium depending on the acoustic impedances of the media (See Section 2.1.2). If the wave transmitted into the second medium is not reflected back later, the energy transmitted can be considered lost.

Refraction of the wave also contributes to higher losses in certain cases because the propagation direction changes (See Section 2.1.2). This is the case when a receiver picks up only a part of the wave or nothing at all, due to this change.

2.8 Backing

To improve the performance of the transducer for diagnostic imaging, a backing material may be applied. During generation of ultrasound, waves will be emitted into the measuring medium, but also internally in the CMUT substrate. This internal resonance will add a ringing effect to the

emitted pulse and increase the duration of the emitted pulse. This leads to a decrease in resolution and also sensitivity since ringing reduces the instantaneous intensity of the emitted pulse[17]. With less instantaneous intensity reflections from poorly reflecting surfaces will not be detectable. It is therefore desirable to add a backing material to absorb the energy in the substrate, and by this reduce ringing, i.e. the number of cycles in the emitted pulse.

For maximum transfer of energy to occur, the acoustic impedance of the backing should be identical to that of the transducer, which can be seen from the relations of reflection and transmission (See Section 2.1.2), where a transmission coefficient at unity would be ideal. The backing material is usually made of an epoxy resin/composite mixed with tungsten powder [17]. This compound's main absorption mechanism is conversion to heat by scattering of the ultrasonic waves by the tungsten particles, as stated by Ph.D candidate Kamal Raj Chapagain. Due to the equal impedances of the transducer and backing material, transmission back into the transducer can occur if the absorption is not great enough. This can be avoided by having a slanted rear side of the backing, which will refract (See Section 2.1.2) the ultrasonic waves away from the transducer [15] [17].

2.9 Transmission line reflection coefficient

A transmission line system can also be looked at as a medium as in Section 2.1 where the load acts as the boundary for an incoming wave. The reflection coefficient (Γ) is still the relation between the reflected and incident wave. These waves can be related to the load (Z) and characteristic impedance (Z_0) of the transmission line by

$$E^+ = Z + Z_0, \tag{2.27}$$
$$E^- = Z - Z_0, \tag{2.28}$$

for the incident and reflected wave respectively. This gives the reflection coefficient

$$\Gamma = \frac{E^-}{E^+} = \frac{Z - Z_0}{Z + Z_0}. \tag{2.29}$$

3. CMUT with backing

One of the goals with this thesis is to do further measurements of those performed in [8] to characterize CMUT behaviour in fluids. Some of the important properties of the CMUT that the measurements should provide information on are center frequency, bandwidth and pulse length.
During the project work done in [8], it was decided to do pulse-echo measurements with rapeseed oil as immersion medium to get the impulse and frequency responses of the system. Rapeseed oil was chosen as the medium because it does not conduct electricity, and has a behaviour that resembles blood which is the medium the CMUT ultimately will operate in. Consequently, values on the properties mentioned above could be calculated, and an evaluation of the CMUT could be done.

An alternative measuring method that could have been used is transmission measurements. In this kind of system there would be two transducers, one CMUT and one standard transducer with known specifications, that would be aligned against each other and immersed in a fluid. One would then act as the transmitter and one as the receiver, and by comparing the emitted and received signals one could have done an evaluation of the CMUT. There are however several difficulties with this type of measurement, with the main ones being alignment, lack of bandwidth in available standard transducers, and possible information loss due to attenuation of the signal through the fluid. Analysis of the data is also more complex since the characteristics of the extra transducer has to be accounted for. Especially ringing in the CMUT could potentially be difficult to evaluate. These problems are less significant in the pulse-echo system since there is only one active element which both simplifies alignment and evaluation of the results. The CMUT also covers its own bandwidth obviously, so the problem with bandwidth coverage is eliminated.

For this thesis, measurements are going to be repeated on the same CMUT, but with the addition of a backing layer on the back side of the CMUT.

This is done to see how a backing layer influences the performance of the CMUT, and hopefully it will produce more unambiguous results than those obtained in [8].

3.1 Method

The pulse-echo measuring system consists mainly of a transducer, a transmission medium, and a reflector. A pulse is emitted by the transducer into the transmission medium, and sent back by the reflector to be received by the transducer. A schematic view of this is shown in Fig 3.1.

The wave will as mentioned in Section 2.7 bleed off energy as it propagates through the transmission medium and at the reflector, and thus will the received wave have less energy compared to the emitted one. This is one of the concerns that have to be accounted for in the analysis of the results.

In order to have a more diverse range of measurements that can be conducted, the system has been set up to be able to precisely adjust the distance between transducer and reflector.

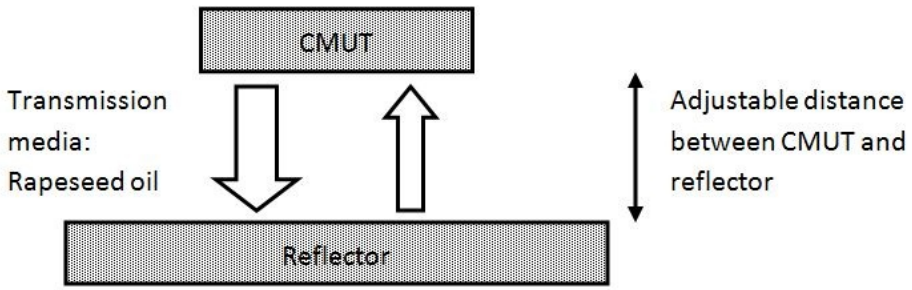

Figure 3.1: Schematic view of the pulse-echo system.

3.2 Devices and equipment

3.2.1 CMUT array with backing

The CMUT array to be characterized by the measurements done in this thesis is a product of the *SMiDA* project. It is, as stated in Section 3, the

same CMUT array as the one measured on in [8], but with the added backing layer on the back side of the array.

This series of CMUT arrays are built up of 57 lines, each consisting of 85 CMUT cells, where the elements have symmetrical interconnections to avoid erratic behaviour of the membrane. All the lines have been connected together in this sample so that it is basically one large element where the active area is $1.275mm \times 0.855mm$, and it has one $100\mu m \times 100\mu m$ connection pad in each corner of the array.

A top down view of the CMUT array and connection pads can be seen in Fig 3.2a, and a zoomed in image of the array showing the symmetrical interconnects is shown in Fig 3.2b. Fig 3.2b also shows the circular membranes, which are placed $15\mu m$ apart center to center, and their top electrodes.

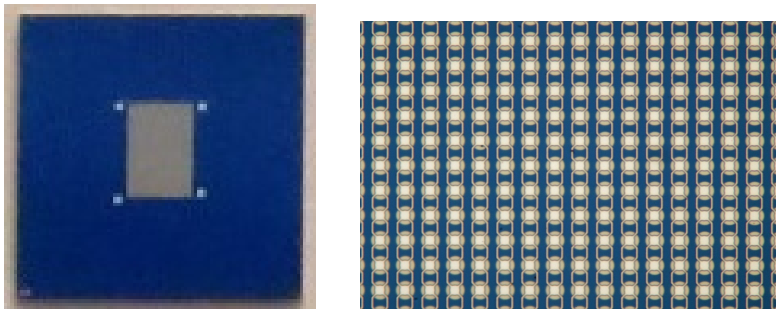

(a) Top down view of the CMUT showing array and connection pads.

(b) Zoomed in view of array showing single CMUT elements and interconnections.

Figure 3.2: Top down views of the CMUT.

The backing material will be added to the backside of the CMUT array. A cross sectional view with dimensions of a single element and backing is presented in Fig 3.3.

For this series of CMUTs it is stated that the collapse voltage will be just above/under $\pm$50V, the resonance frequency in air is about 36-37 MHz, and the center frequency in immersion is expected to be around 10-12 MHz. All values on dimensions and properties stated in this section were verified by Ph.D. candidate Sigrid Berg and Ph.D candidate Kjersti Midtbø.

The backing layer is made of a two component epoxy compound mixed with tungsten powder to a concentration of about 30%. The epoxy used is EPO-TEK 301 from Epoxy Technologies, and the tungsten powder consists mainly of particles of 1 and 5 μm in size. The thickness of the layer

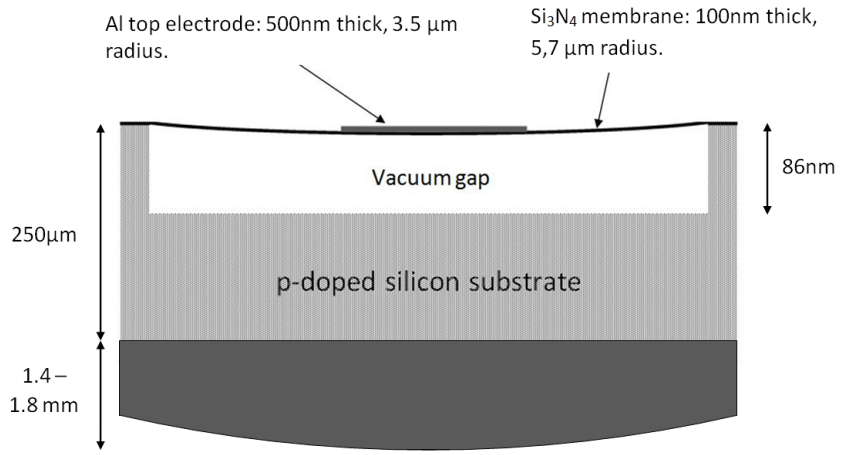

Figure 3.3: A cross sectional schematic of a single CMUT element and backing, with dimensions (Not to scale).

is about $1.8mm$ at its center, and it has a curved backside which ends at $1.4mm$ at the sides where it meets the PCB. This curved backside formed during curing, probably due to surface tension and expansion of the epoxy mixture.

3.2.2 Bias-T PCB, and connections

The primary functions of the bias-T printed circuit board (PCB) are to have a mounting surface for the CMUT, and to add the AC and DC components that drive the CMUT. It also protects the measuring equipment and signal generator from harmful DC currents.

The bias-T used for these measurements uses only a resistor and a capacitor to provide this capability. A schematic drawing of the bias-T is shown in Fig 3.4. The values of the resistor R and capacitor C are $1M\Omega$ and $1nF(100V)$ respectively, which are the same values used in an earlier experiment on similar CMUTs reported in [21].

The bias-T PCB was made as part of the work in [8], and an image of it with the resistor and capacitor soldered on is shown in Fig 3.5. The PCB was fabricated with two holes, where the center hole provided the option of adding a backing layer for the measurements in this thesis. The resistor and capacitor used are from the 1206 surface mounted component (SMC) package, which are small enough so that they would not be a hindrance to the range of distances the CMUT could be placed from the reflector.

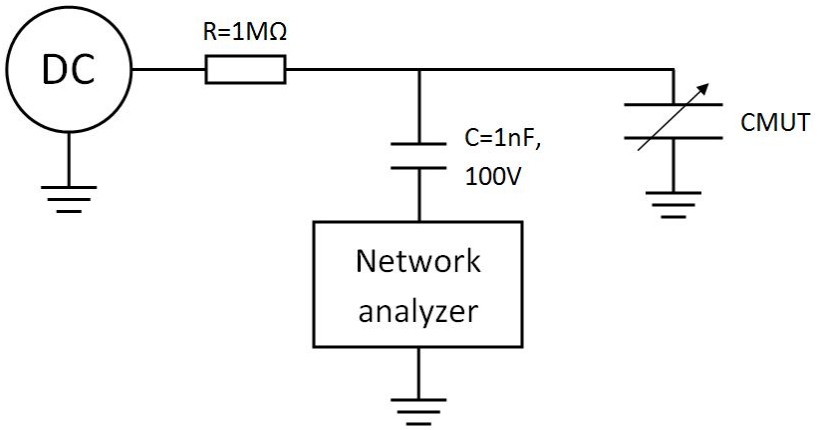

Figure 3.4: Schematic drawing of a bias-T.

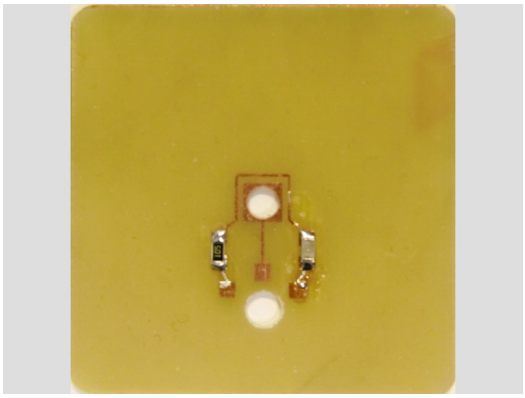

Figure 3.5: The PCB with resistor and capacitor mounted.

Fig 3.6 shows the fully assembled PCB with signal cables, and Fig 3.7 shows the back side with the center hole filled with the backing layer. The CMUT was mounted to the board using silver glue to make a good connection to ground, and the pads were connected to the signal line by gold wire bonding. This bonding proved to be difficult on the copper lines, so silver glue had to be used to strengthen the connection.

The signal cables chosen were of the type RG 174 due to their size and flexibility in addition to shielding, and they were terminated with BNC connectors to fit the equipment in the laboratory.

Adding the backing layer was fairly easy as the tape covering the center hole of the PCB had kept the oil out during the initial measurements without backing. As the hole and backside of the CMUT were clean, the epoxy tungsten compound was filled directly into the hole onto the back of the

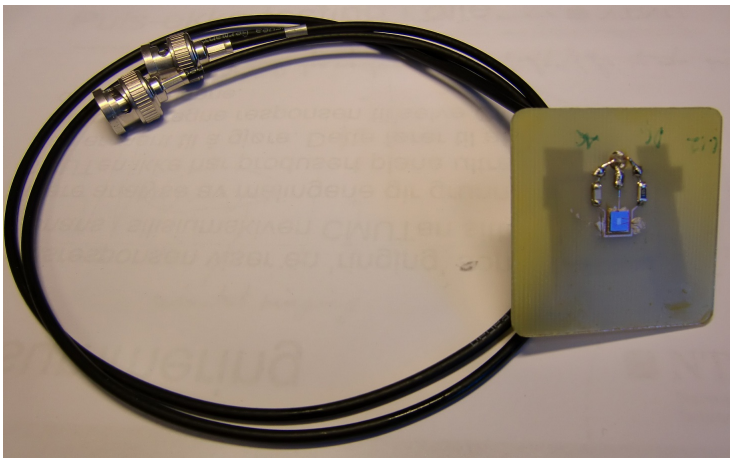

Figure 3.6: Fully assembled PCB with signal cables.

CMUT, and then left to cure over night.

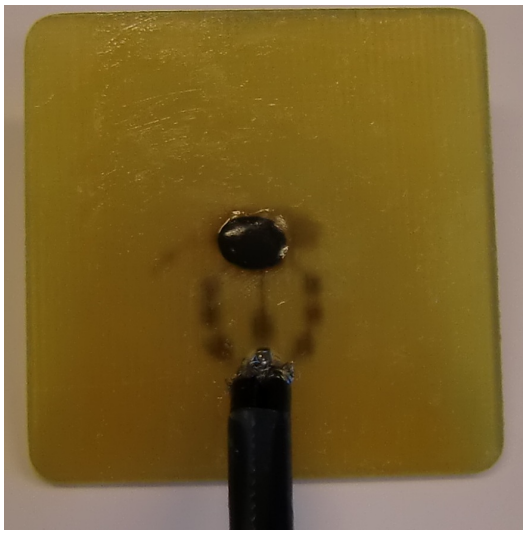

Figure 3.7: Back side of the PCB showing the center hole filled with the backing layer.

3.2.3 Pulse-Echo Rig

The pulse-echo rig consists of a mounting plate for the PCB, a $10mm$ thick steel base that seconds as the reflector of the system, and a mechanism for adjusting the distance between the mounting plate and the reflector surface. Images of the rig is shown in Fig 3.8.

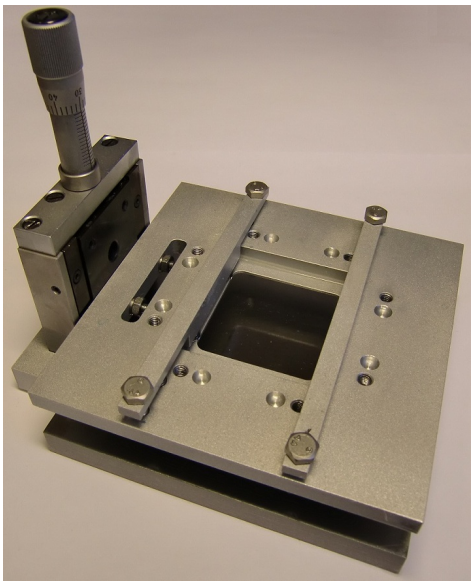

(a) Pulse-Echo Rig without PCB.

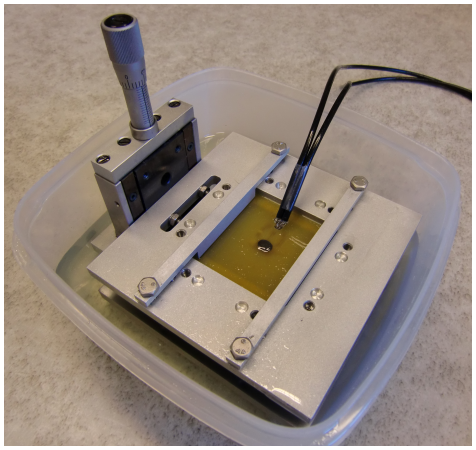

(b) Immersed Pulse-Echo Rig with PCB.

Figure 3.8: Pulse-Echo Rig.

The aluminium mounting plate has a window that the PCB is placed in so that the CMUT faces the reflector, and the PCB is kept in place by two spring loaded beams that are screwed to the plate. The PCB also rest on a set of springs and can therefore be angled somewhat to adjust alignment with the the reflector.

Precision adjustment of the distance between CMUT and reflector is needed. The mechanism used on the rig was originally intended for use in optical measurements, and can adjust the distance with a precision of about $10 - 20\mu m$.

In order for the steel base to function as a reflector it has to have a surface that does not influence and cause distortions of the measurements. Professor Arne Rønnekleiv stated in a *SMiDA* group meeting that a tolerance comparable to Δ given in (3.1) should be sufficient. This is a dimension commonly used for optical experiments that also holds for ultrasonics.

$$\Delta = \frac{1}{10}\lambda, \tag{3.1}$$

$$\Delta = \frac{1}{10}\lambda = \frac{1}{10} \cdot \frac{1445m/s}{30 \cdot 10^6 Hz} = 4.81\mu m \approx 5\mu m. \tag{3.2}$$

Calculating for 30MHz and assuming that the speed of sound in the oil is $1445m/s$, a tolerance of $5\mu m$ was obtained as shown in equation (3.2). Measuring results from [8] indicate that the actual speed of sound in the medium is closer to $1460m/s$. This confirms that the tolerance holds since the difference between the assumed and actual value is small.

Another crucial property of the reflector is that its transmission coefficient should be as low as possible in order to avoid unnecessary signal loss. The formula for calculating the acoustic impedance of a medium is

$$Z_{acoustic} = \rho \cdot c, \tag{3.3}$$

where ρ is the density of the medium and c is the acoustic propagation velocity. Using equation (3.3), with the density of rapeseed oil given in [22] and the velocity found from measurements in [8], gives an acoustic impedance of

$$Z_{Oil} = 910\frac{kg}{m^3} \cdot 1460\frac{m}{s} \approx 133 \cdot 10^4 \frac{Pa \cdot s}{m}. \tag{3.4}$$

The acoustic impedance of steel is in [15] given as: $46.3 \cdot 10^6 Pa \cdot s/m$. By using these values in equation (2.5) the result is

$$D = 1 - \left(\frac{Z_{Steel} - Z_{Oil}}{Z_{Steel} + Z_{Oil}}\right)^2 = 0.1, \tag{3.5}$$

which means that it should work as a good reflector with a reflected wave intensity of 90% compared to the incident wave. A secondary reflection from the bottom surface of a reflector can occur. However, with the transmission coefficient for these media, its intensity will be 100 times smaller from reflection and transmission losses alone, and can for all practical purposes be neglected.

3.2.4 Network analyzer

A network analyzer was used to both drive and measure the signal from the CMUT. It can do single channel pulse-echo testing with sweeps over large frequency spans, and is therefore an effective tool for testing CMUTs.

The majority of the testing was done on the Rohde & Schwarts (Vector Network Analyzer 10Hz/9kHz-...4GHz), because of its ability to switch

between frequency and time domain, and its time gating capability. This reduces the data processing required during analysis, since it can for example set a time gate around a single echo and produce its corresponding frequency response directly.

Some inconsistencies were encountered in measurements done with the Rohde & Schwarts, and therefore a HP8753E network analyzer was used to check and correct these abnormalities.

3.2.5 Test setup

The complete setup ready for immersion testing is shown in Fig 3.9. The bias voltage from the DC source was controlled by a multimeter to insure that it had the correct value.

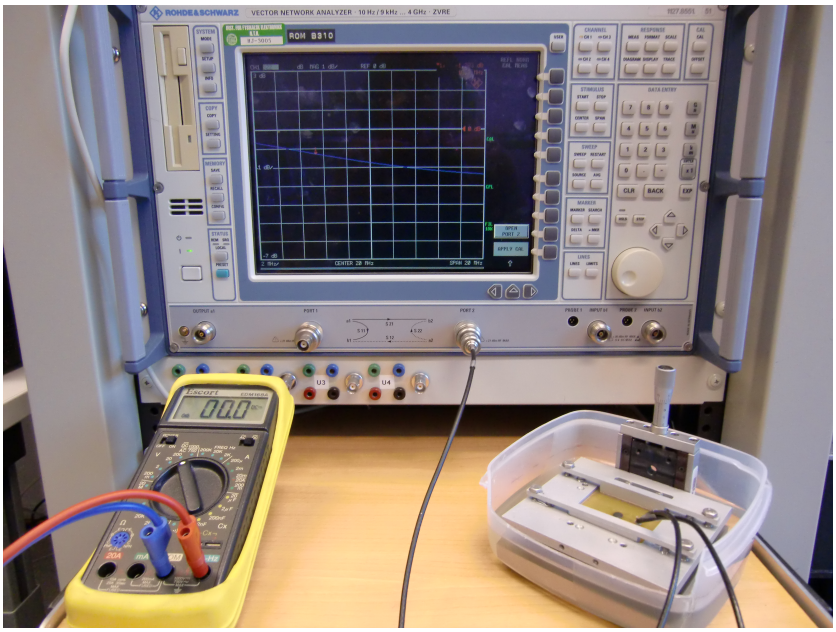

Figure 3.9: Complete setup for immersion testing with the Rohde & Schwarts network analyzer. Bias voltage source is not visible.

3.3 Pulse-echo testing

For this pulse-echo test, the rig was placed in a plastic box as shown in Fig 3.9, and rapeseed oil were added so that the CMUT and PCB was com-

pletely immersed.
Care had to be taken to ensure that the surface of the CMUT were devoid of any air bubbles that could distort the measurements. The rig was therefore placed at an angle in the box so that trapped air could drift of the CMUT, and escape through the wire hole in the PCB or at the board edge. Due to the viscosity of the rapeseed oil, the setup was left like this for some time to allow the air to escape and the oil to settle.

The PCB was mounted in the holder and checked with a slide caliper to make sure that it was properly aligned with the reflector, and to make sure it was placed in the same position as in [8]. This was because it was believed to give the best response, and to simplify comparison during the analysis of the results.
Due to the process of gluing the CMUT to the PCB, some misalignment is expected even if the PCB is aligned with the reflector. A sample used for gluing practice were checked to see how skewed the CMUT can be expected to be. The measurement showed the deviation to be at most $2.5\mu m$ over $1mm$, and this suggested that manual alignment to get a better response would not be feasible.

With the holder all the way down on the reflector, the distance up to the CMUT was found to be $0.9mm$. This was based on the dimensions of the rig, the measured height of the CMUT and the glue on the sample used for gluing practice, and is therefore subject to some uncertainty.

The testing started of by varying the bias voltage between -0V and -45V, to check for irregularities compared to its behaviour from the tests in [8] .
The main test series were done with a frequency sweep from 1MHz to 50MHz and a signal power of -25dBm. A bias close to the collapse voltage of the CMUT gives, according to (2.20) and (2.22), the greatest signal intensity, and thereby the clearest response. For these measurements however, collapse have to be avoided and the bias is therefore set to -45V. The series were performed at distances of $1.4mm$ and $1.9mm$ between the reflector and the CMUT.

4. Rapeseed oil attenuation

When performing characterization measurements, whether it is pulse-echo, transmission measurements or others, the initial results one will obtain is characteristic for the system as a whole, and not for the tested device itself. In order to get a better impression of the performance of the tested device, variables in the system will have to be accounted and compensated for.

Attenuation in the measuring medium is one of the main variables that affect the initial result, especially since it varies as a function of frequency (See Section 2.7.1). Finding the attenuation of the medium that the measurements are performed in, in this case rapeseed oil, is therefore needed to produce a normalized response curve for the CMUT.

From equation (2.25) a fairly precise theoretical value for the attenuation can be calculated. In the data on the rapeseed oil provided by the Department of Biotechnology at NTNU, a value for the volume viscosity is not stated. This means that equation (2.24) has to be used, and this is suspected to give smaller values than the actual ones as stated in Section 2.7.1. A measurement of the attenuation is therefore needed to produce a correction curve, and not only for validating and adjusting a theoretical one.

4.1 Method

For measuring the attenuation, pulse-echo measurements similar to those presented in Section 3 have been performed. This meant having a transducer emitting and receiving a wave that is reflected by a steel block, while propagating through rapeseed oil. The reason for choosing pulse-echo measuring was mainly equipment availability and familiarity, but the advantages presented in Section 3 also applies here. The main difference

in the system is that instead of using the CMUT, a set of commercial ultrasound transducers were used to transmit and receive the ultrasound waves. This was because these transducers have a known characteristic, and this excludes uncertainties like electrical mismatches and other unknown factors that may be present in the CMUT. A drawback with these transducers is the relatively narrow bandwidth that they operate with. This meant that several transducers had to be used in order to cover a wide enough range of frequencies.

4.2 Devices, equipment and execution

4.2.1 Olympus Panametrics-NDT ultrasound tranducers

The transducers used are from the Olympus Panametrics-NDT V300 series, which are made for immersion use. These transducers come with a variety of different center frequencies, have a 1/4 wavelength element of 0.25" in diameter, and a 6 dB bandwidth between approximately 50% and 100%. A selection of transducers with center frequencies ranging from 5MHz up to 30Mhz have been chosen to cover the frequency range of the CMUT measurements.
The 30 MHz transducer has a delay line of fused silica at its front to protect its piezoelectric element. Fused silica has an acoustic impedance that poorly matches water, as stated in [23], and it is therefore expected to give reflections at the transducer/oil interface. The specific characteristics of the individual transducers are presented in Appendix A.

4.2.2 Reflector

Since these measurements are done in the same frequency range as the CMUT, the steel base of the pulse-echo rig was chosen as the reflector.
A problem with this was that the available plastic box to place the rig in did not give it a flat surface to rest on, and thereby making it difficult to level out the rig which would have been preferable for alignment with the transducer. It was however considered to be a manageable difficulty, since the setup in any case required manual alignment of the transducer relative to the reflector.

4.2.3 Network analyzer

The Rohde & Schwarts (Vector Network Analyzer 10Hz/9kHz-...4GHz) was used to drive and perform the measurements.

As pointed out in Section 3.2.4, this network analyzer can switch between frequency and time domain. This is very useful for these kind of measurements since it presents both responses during testing, and thereby making transducer alignment and data gathering easier. This results in more effective testing due to reduced data processing and that problems can be identified and avoided.

One drawback with this network analyzer is that its only functioning port delivers maximally 0dBm of power to its load. The v300 series tranducers however are rated for a maximum of 125mW($\approx$21dBm) [23], and the low output of the network analyzer might therefore produce pulses of limited intensity. This could result in a poor signal to noise ratio in the measurements.

4.2.4 Test setup and procedure

The complete setup for the attenuation testing is shown is Fig 4.1. A standard laboratory holder is used for transducer fixation, and manual alignment is therefore required. Beyond that, it is basically the same as the setup for testing the CMUT, with the exception that these transducers operate on an AC source alone.

Two methods have been used for measuring the attenuation in the oil. The principle of the first method was to measure the magnitude of the first received echo at a given frequency, and for two different distances from the reflector.

A transducer with frequency band covering the frequency of interest was placed in the holder and lowered into the oil. It was then checked visually for air bubbles on the front of the transducer, and measures were taken to remove these if present.

Before connecting the network analyzer to the transducer, its frequency sweep range and power had to be set, and a calibration for these settings had to be performed. An appropriate frequency sweep corresponding to the center frequency of the chosen transducer was set, and power delivery of the network analyzer was set to its maximum of 0dBm. A calibration

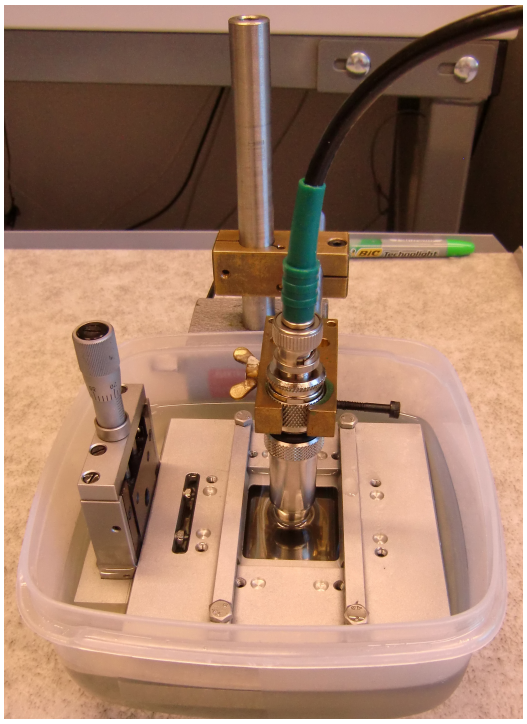

Figure 4.1: Complete setup for rapeseed oil attenuation testing.

was then performed to remove the influence the connection cable had on the response with these settings.
As part of the last preparations before measuring could be carried out, the position of the holder arm and through this, the position of the transducer was measured with a slide caliper. This gave a reference position with a precision of $\pm 50 \mu m$.

Alignment of the transducer relative to the reflector was done by sweeping it around one axis at a time and checking the response on the network analyzer. Both frequency and time domain modes were monitored in order to obtain the most precise alignment, and to identify and correct any irregularities in one mode if present. After sweeping both axes the transducer was fixated in the position where the greatest response magnitude was obtained.

The measurements themselves were done by using the network analyzer's time gating feature to single out the first echo in the time domain, and then display its frequency response. The magnitude of the response at the frequency in question could then be acquired.
After the first measurement was completed, the holder was set to a new

position, and measured again with the slide caliper to get the new reference position.

The procedure was then repeated for the remaining transducers to cover the whole frequency range.

Calculating the attenuation (α_{freq}) for a given frequency was done using equation (4.1).

$$\alpha_{freq} = \frac{M_1 - M_2}{2(P_1 - P_2)}, \tag{4.1}$$

where M_1 and M_2 are the magnitudes at positions P_1 and P_2 respectively. The factor 2 in the denominator is present because the sound travels the distance measured twice going to and from the reflector.

For the second method the preparations before measuring were the same as for the first one. The difference between the two is that instead of moving the holder to a new position as in the first one, the second echo is used in this one. By time gating and measuring both the first and second echo at a given frequency, the attenuation can be found using equation (4.2).

$$\alpha_{freq} = \frac{M_2 - M_1}{c(T_2 - T_1)}, \tag{4.2}$$

where M_1 and M_2 are the magnitudes, and T_1 and T_2 are the placements in time of echo 1 and 2 respectively. The factor c denotes the propagation velocity of the oil.

4.3 Theoretical and measured attenuation

4.3.1 Theoretical rapeseed attenuation

A theoretical value of α_0 was calculated using (2.24), multiplied with the conversion factor for dB (2.26), and the following values:

- Dynamic viscosity, $\eta = 72.1mPa \cdot s$.
- Density, $\rho = 910kg/m^3$.
- Propagation velocity, $c = 1460m/s$.

This results in

$$\alpha_0 = 5.811 \cdot 10^{-12} \frac{dB \cdot s^2}{m}, \tag{4.3}$$

and hence equation (2.24) produces the relation between attenuation and frequency presented in Fig 4.2.

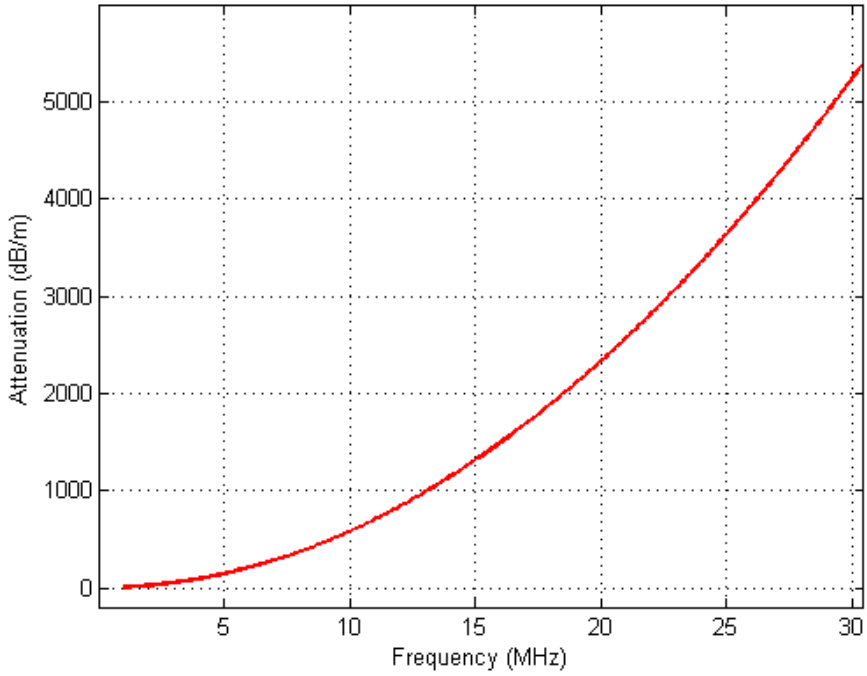

Figure 4.2: Theoretical attenuation versus frequency.

4.3.2 Measured rapeseed attenuation

Each of the methods have their weaknesses that can be a source of uncertainty in the measurements.
The source of greatest uncertainty in the first method is when the transducer is moved to a new position. This might lead to a skewed alignment of the transducer, and the measurement of the two positions are also subject to some uncertainty.
The propagation speed c is the source of greatest uncertainty in the second method. It was found by measuring the placement of the first echo in time

at two different positions, and is thus subject to uncertainty as mentioned above.

The measurement series were performed six times for each method to have a set of values to average over. This was done to even out the uncertainties of the measurements. The averaging was also weighted, meaning that the largest deviations were essentially excluded. The system is inherently lossy, and the measurements with the lowest losses can therefore be considered to be closer to the real value than those with higher values. This does not mean that picking out the lowest value for each frequency will be acceptable, since for example a value for c that is too high gives attenuation values that are too low. Both methods gave values in the same range of attenuation values for each frequency, and they were therefore processed together in the calculation of data points.

Fig 4.3 shows the plotted data points representing the averaged values for specific frequencies, and the adapted curve for the attenuation as a function of frequency. More weight have also been put to the lower frequencies since the attenuation is lower here, and measuring errors will have less effect compared to the higher frequencies. The significance of this can be seen in Fig 4.3 where the curve follows the lower frequency values closer compared to the values at higher frequencies.

This corresponds to $\alpha = \alpha_0 f^2$ with

$$\alpha_0 = 7.5 \cdot 10^{-12} \frac{dB \cdot s^2}{m}, \tag{4.4}$$

which is about 1.3 times greater than the theoretical value of α_0.

During the measurements with the 10MHz transducer, the received magnitude was initially recorded at its peak frequency of 11.92MHz. During one of the series however, the magnitudes were recorded at 10MHz by mistake. Instead of rejecting this series, this was repeated 5 times to be used as the extra data point seen in Fig 4.3.

Measuring with the 30Mhz transducer proved to be to difficult to produce any valid results. The reason was the fused silica piece, mentioned in Section 4.2.1, combined with the low output power from the network analyzer (See Section 4.2.3). This combination produced a result where the echoes from the reflector drowned almost entirely in the reflections from the transducer/oil interface, making the response too noisy to be used.

The actual attenuation turned out to be higher than the theoretical value,

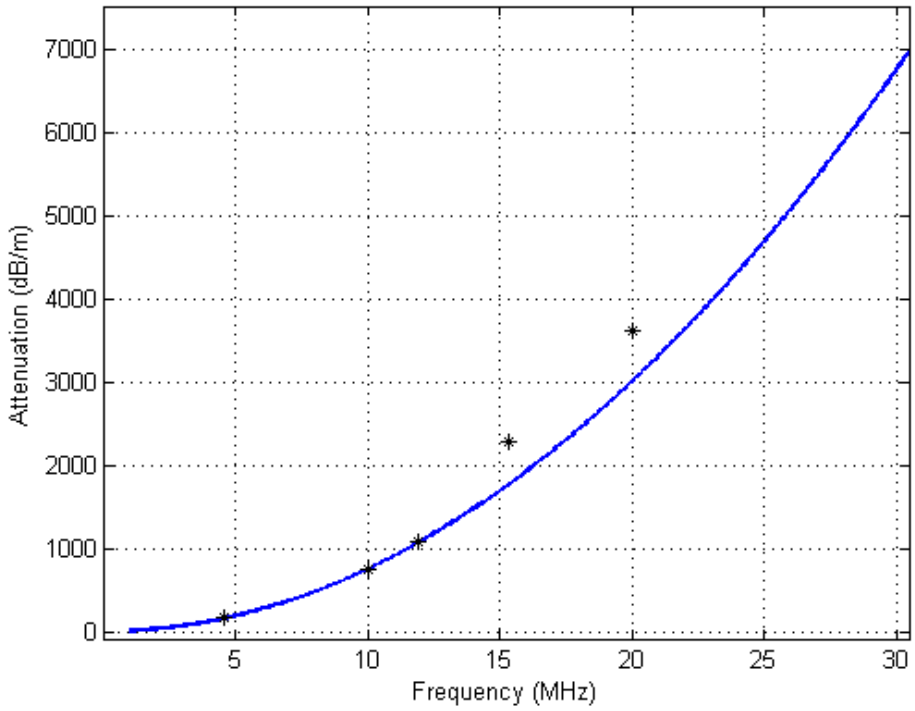

Figure 4.3: Averaged data points and adapted curve for the measured attenuation versus frequency.

as expected from the theory presented in Section 2.7.1. The result is also a comparable value with the results presented in [22] and [24], on similar vegetable oils.
The main source of the increased attenuation, compared to the theoretical one, is probably the effects added by the volume viscosity, assuming the oil is homogeneous. It is however unlikely that the oil is completely free from some undissolved cells or other impurities, so scattering may be a contributor too.

5. Results and discussion

This section contains key plots of the results, and discussion of these, from the measurements described in Section 3.
This section is divided into three parts where Section 5.1 contains the analysis of the performance of the added backing layer, and Section 5.2 covers the general behaviour and key features of the CMUT. Section 5.3 discusses an adapted impedance network for the system.

All of the data presented in this section is a product of processing in MATLAB, and any stated values have also been found through this process. It should be noted that the plots taken from [8] presents the data in Hz and seconds, while the rest are in MHz and μs.

5.1 Backing layer performance

The CMUTs manner of operation in relation to the applied bias voltage were observed qualitatively before conducting these measurements. Equation (2.22) suggests a greater output for an increasing bias voltage, and it was found in [8] that the CMUT followed this pattern. As this was already established for the CMUT, the observation served to confirm that the CMUT functioned properly, and still followed this pattern after the addition of the backing layer.

The purpose of the backing layer is to reduce the ringing effect in the CMUT. This has been reported to be effective in [9], and comparison with measurements from before the layer was added will show how it performs in this case.

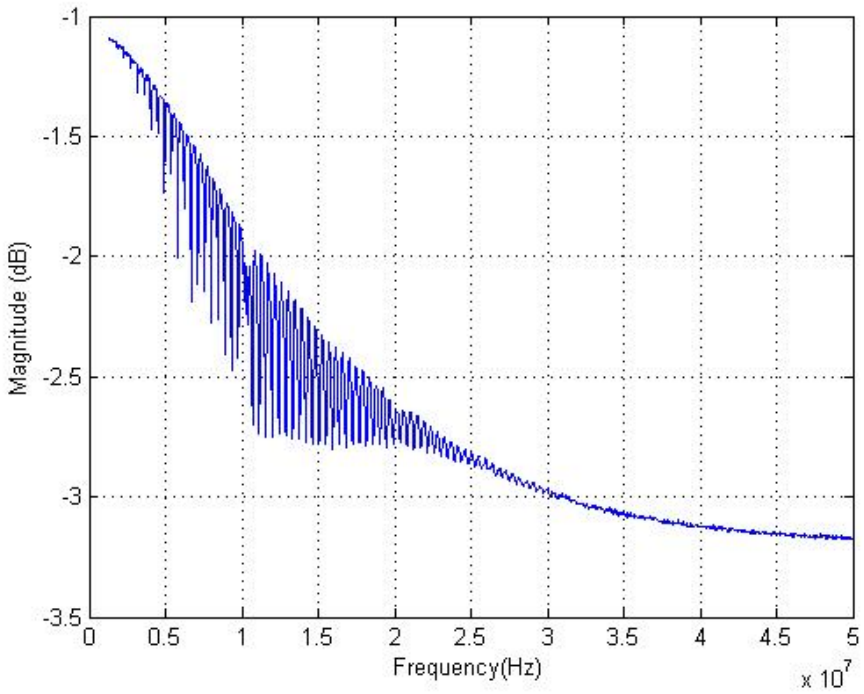

Figure 5.1: CMUT frequency response in immersion without the backing layer, at -45V bias voltage and a distance of 1.4mm to the reflector (from [8]).

The initial frequency responses for the CMUT, without and with the backing layer added, are shown in Fig 5.1 and Fig 5.2 respectively. The ripple in the response is expected in both cases, and corresponds to the distance

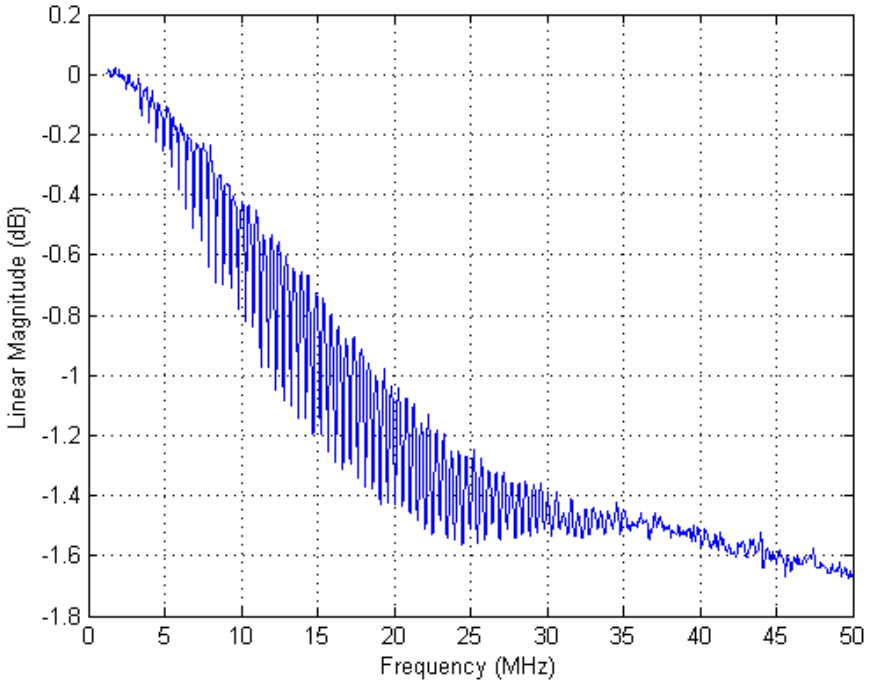

Figure 5.2: CMUT frequency response in immersion with the backing layer, at -45V bias voltage and a distance of 1.4mm to the reflector.

from the reflector and the speed of sound in the rapeseed oil. The property of interest in these plots is a dip in the magnitude of the ripple, as the one seen at about 10MHz, and less notable at about 20MHz in Fig 5.1. These are believed to be appearing due to ringing, as similar behaviour were reported in [9] and [25].
In the response with the backing layer added these dips are much less prominent, which indicates that the layer dampens the ringing. The maximum magnitude of the ripple is also lower as would be expected with the dampening, but there is a greater response from 20MHz up to about 30MHz. This is unexpected as the backing layer is a passive component, which means that other alterations to the CMUT may have occurred.

Fig 5.3 shows the impulse response of the system with the backing layer. The first echo is clearly visible at $2.05\mu s$, which means that the distance (D) between the CMUT and reflector is quite accurate as the calculation in equation (5.1) shows.

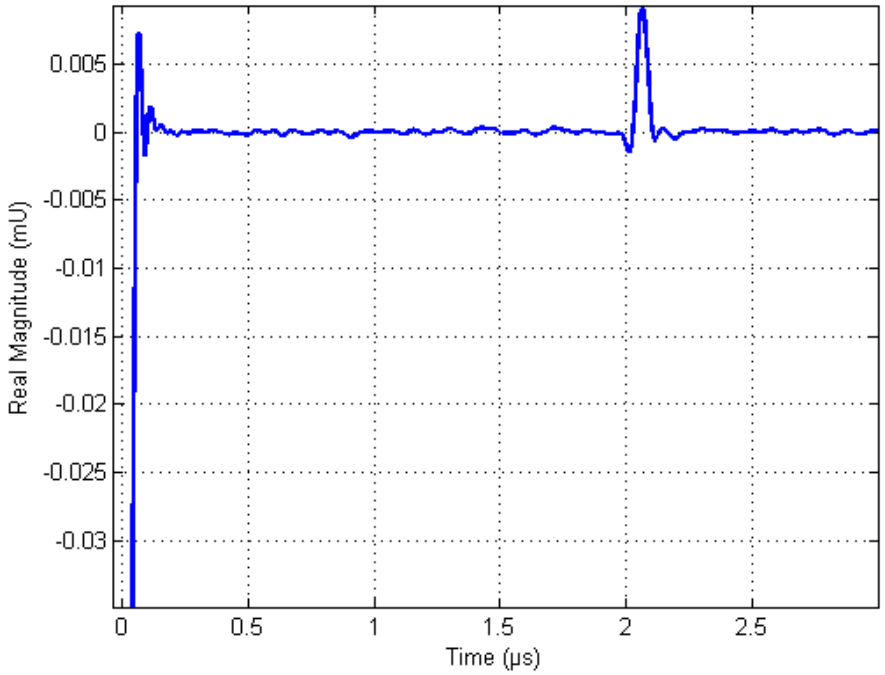

Figure 5.3: Trimmed impulse response with first echo at 1.4mm from the reflector.

$$D = 1460\frac{m}{s} \cdot 2.05\mu s = 2.9mm, \tag{5.1}$$

which gives a deviation of $0.1mm$ without taking time losses in the measuring system into account.

A zoomed in section of the first echo for the CMUT, with and without the backing layer, is showed in Fig 5.5 and Fig 5.4 respectively.
A ringing motion after the echo can be observed in Fig 5.4. This ringing has a period of $0.065\mu s$ which is comparable to

$$T = 2t/c_{Si} = \frac{2 \cdot 250\mu s}{8400m/s} = 0.06\mu s, \tag{5.2}$$

where t is the thickness of the CMUT chip, and c_{Si} is a general propagation velocity of sound in silicon. This confirms that the ringing is resonance internally in the CMUT chip as suspected in relation to [9] and [25].
Comparing with Fig 5.5 shows that the backing layer has a considerable dampening effect, resulting in as good as total diminishing of the ringing.

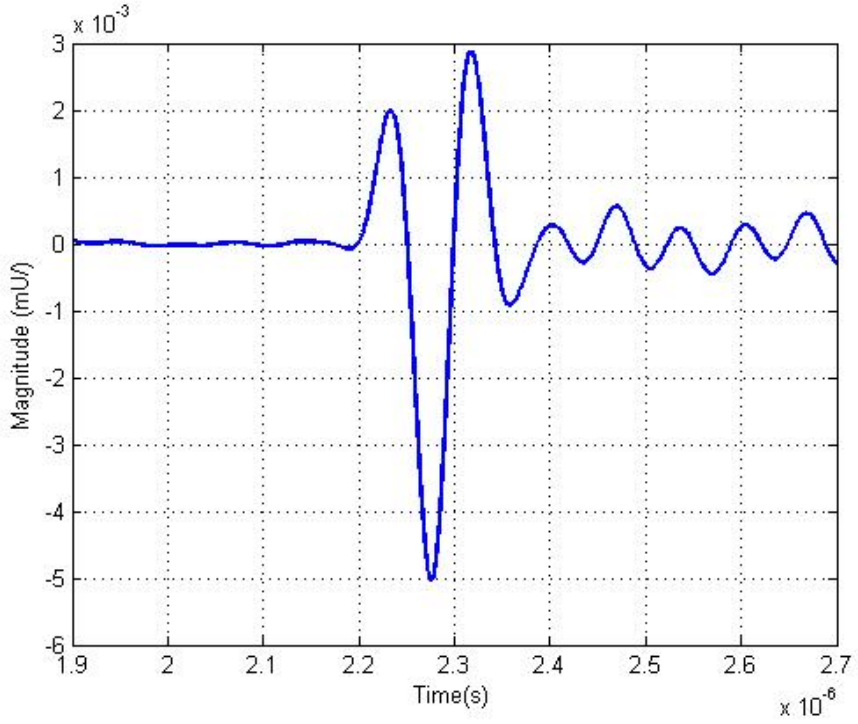

Figure 5.4: Zoomed in impulse response of the first echo, without backing layer (from [8]).

Even though the ringing has been removed, other disturbances can appear in effect of the added backing layer as described in Section 2.8. Examples are disturbances due to reflections from the CMUT/backing layer interface because of poor acoustic impedance matching(See Section 2.1.2), or reflections from the end of the backing layer returning to the CMUT.
The first case can be considered unlikely in this case, since reflections in the CMUT/backing layer interface would cause a persisting ringing.
Reflections from the end of the backing layer is not unlikely as this interface was with air, and therefore a great acoustic impedance mismatch. This will however only occur in the case where the acoustic dampening of the layer is too small to absorb all of the energy transferred to the layer. The sound propagation velocity in the EPO-TEK epoxy is stated in [26] to be $2650m/s$, and the thickness of the backing layer is varying from $1.4mm$ at the edges to $1.8mm$ at the center. This gives

$$T = 2t/c_{EPO-TEK} = 1.06\mu s \Leftrightarrow 1.36\mu s. \tag{5.3}$$

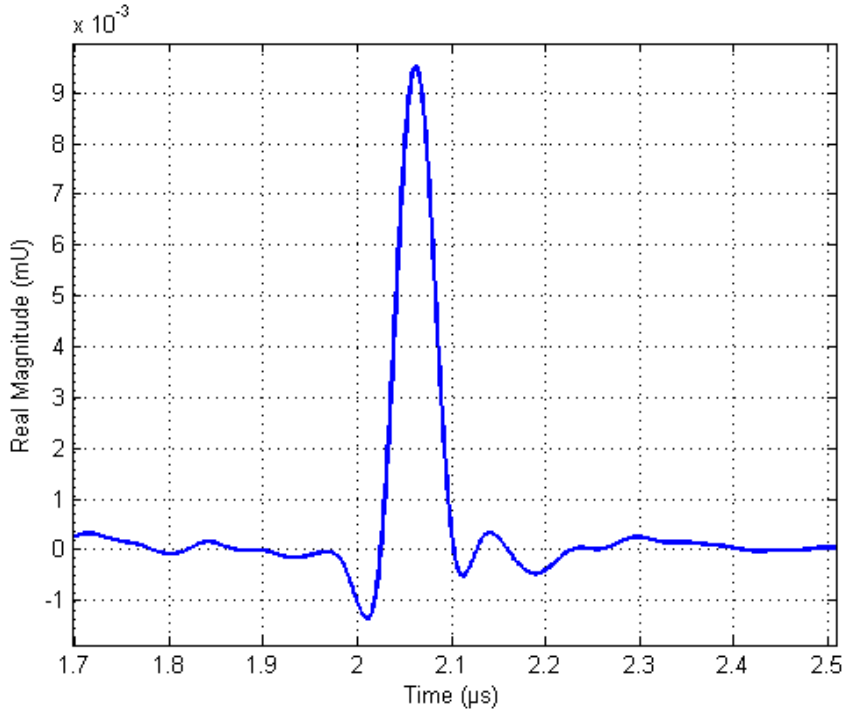

Figure 5.5: Zoomed in impulse response of the first echo, with the added backing layer.

In this time interval after the echo, only the same rather random noise seen in Fig 5.3 and Fig 5.5 is present. It can therefore be concluded that the backing layer absorbs all the energy transferred from the CMUT. For a transducer to be used for imaging, this grade of absorption may be too much as this degrades the transducer sensitivity according to [27] and [17]. On this type of transducer with the backing layer added to its back side, this degradation is of less concern as it would take a very high grade of dampening to have much effect, as stated by Professor Rønnekleiv. For this case it works well regardless of any degradation, and also serves as a proof of concept.

5.2 General performance

The evaluation of the CMUTs general performance were, as mentioned in the introduction (Section 1), inconclusive in [8]. The irregular behaviour observed in the results was believed to be due to increased line resistances

and capacitances, as a result of poor bonding connections. This increase might have caused phase shifts over the array leading to an uneven output that produced the poor results.

In an effort to get a better impression of the CMUT performance, and to try to verify the source and severity of the problem, normalization of the results has been done. A measure of the rapeseed oil attenuation was found in Section 4, and can thus be compensated for in the results.
Another factor that should be accounted for in these types of measurements is divergence of the ultrasound beam. For this particular case however, this is a factor of less concern because the distance the sound travels does not extend beyond the near field depth (NFD) for most of the emitted frequencies. A quality of the near field is a constant beam width, but it does exhibit a varying intensity due to interference. For this case however, the intensity should be stable since the CMUT is a broadbanded transducer, and therefore have a lot of different frequencies that interfere. Using equation (2.8) with $b = 1.275mm$, and the wavelength for the oil at 10MHz yields

$$FF > \frac{1.275mm^2}{2.88 \cdot 0.29mm} \approx 3.9mm. \tag{5.4}$$

This is about the same as the distance the sound has traveled with the CMUT placed $1.9mm$ from the reflector. The significance of this is that only frequency components lower than 10MHz will be subjected to divergence, and it is therefore expected to be of little effect to this analysis.

As Fig 5.6 shows, the attenuation being related to the square of the frequency means that it affects the measured response quite a lot. The combined plots of the compensated responses of the first echo from positions $1.4mm$ and $1.9mm$ are shown in Fig 5.7. These plots indicates that the value found for the attenuation is fairly accurate since the curves are placed almost on top of each other, at least for the fairly stable area from 10MHz to about 25MHz.

The air testing performed in [8] showed a peak frequency of 36MHz. When the CMUT is immersed this is expected to shift to a much lower value. It has been stated by Professor Rønnekleiv that the peak frequency should be in the area of 10 to 12MHz for this CMUT design when immersed. The results presented in Fig 5.6 and Fig 5.7 does, with this in mind, seem to be quite far off from this expectation.
The addition of the backing layer was hoped to give a more stable response

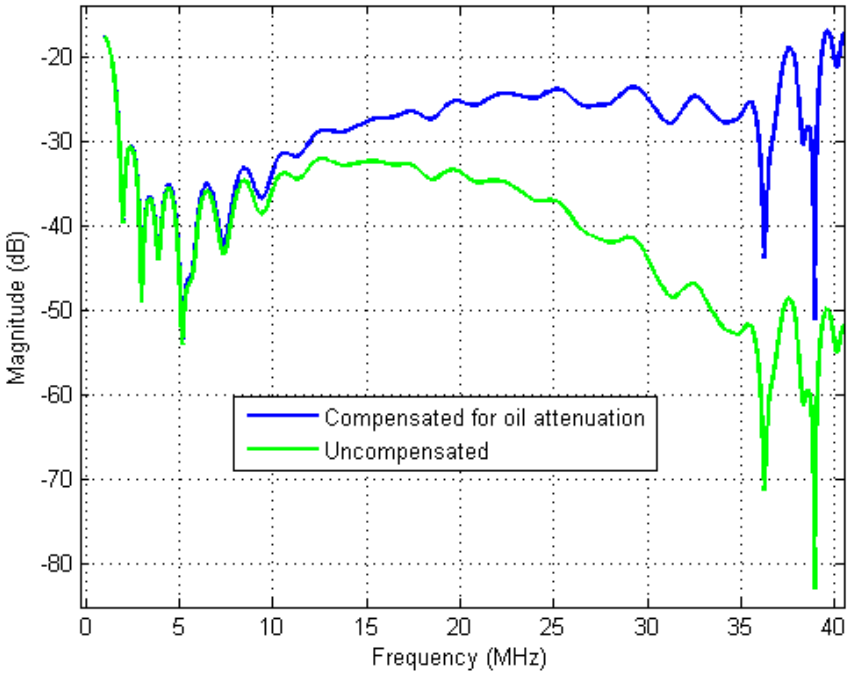

Figure 5.6: Compensated and uncompensated frequency response for echo 1 at a distance of 1.4mm.

from the CMUT, but it is quite evident seeing the results that this is unfortunately not the case. Finding characterization properties like center frequency and bandwidth are therefore not possible through these plots.
These responses have a good resemblance with those procured in [8], but there are some differences. Comparing the responses of the first echo at $1.4mm$ in Fig 5.6 and Fig 5.8, shows that the response when the backing layers are added actually has more distortions than the one without backing. It also shows that the response with backing does not drop off as much as the one without, as the frequency increases. This supports the suspicion of an unknown alteration to the CMUT, together with the observation of the increased response from 20MHz to about 30MHz in Fig 5.2.

The observations mentioned above indicates a shift in resonance frequency of the CMUT to a higher one. Looking at equation (2.23) the most likely parameters to be affected by an external addition to the CMUT are, an effective increase in the thickness (t) of the membrane, or an increased membrane spring constant (k_{mem}) by an increase in membrane tension.

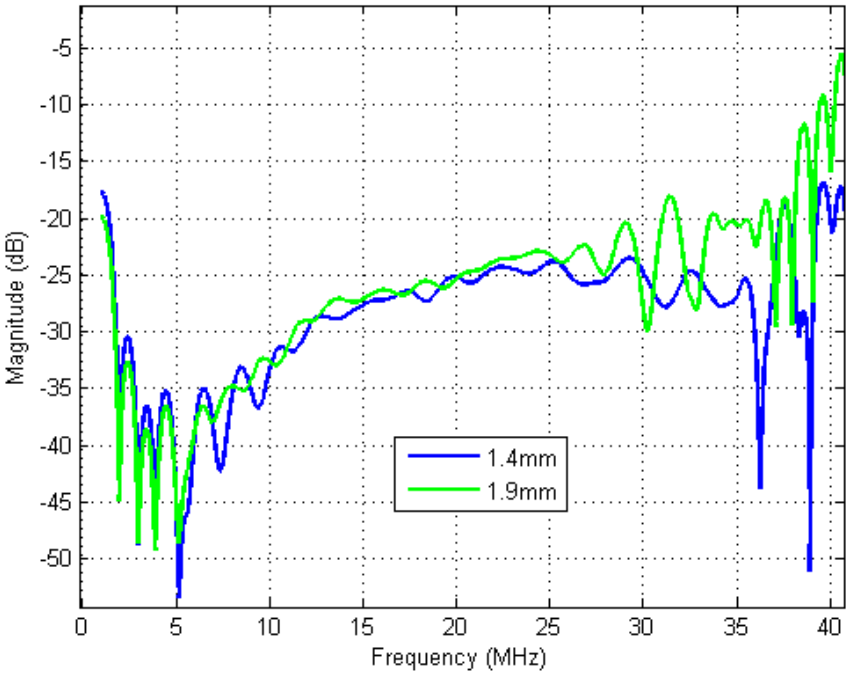

Figure 5.7: Combined plot of compensated frequency response for the fist echo at both 1.4mm and 1.9mm.

The only substance the CMUT have been subjected to that can affect the membrane thickness is the rapeseed oil. After the completion of the autumn project [8], the CMUT was left out in air to dry off. It could not be cleaned due to its fragile exterior and the bonding leads connected to it. This allowed a layer of oil to remain on the surface of the CMUT, and eventually set on it. This could perhaps increase the effective thickness of the membrane, the CMUT was however mounted in the rig and immersed and left like this for about half a day. The probability that the dry layer of oil did not dissolve during this period is small, as it dissolved on all of the surfaces of the pulse-echo rig that were treated in the same way.

This leaves the increase in spring constant (k_{mem}). The membrane is fixated in a span between the support structure fabricated in the silicon substrate, and is thus subject to tension in this structure.
The CMUT chip is glued to the PCB. When the backing epoxy mixture was added, this was poured into the hole in the PCB, and left to cure. During the curing process, expansion or shrinking of the epoxy volume is not uncommon. This type of change can affect the CMUT, resulting in

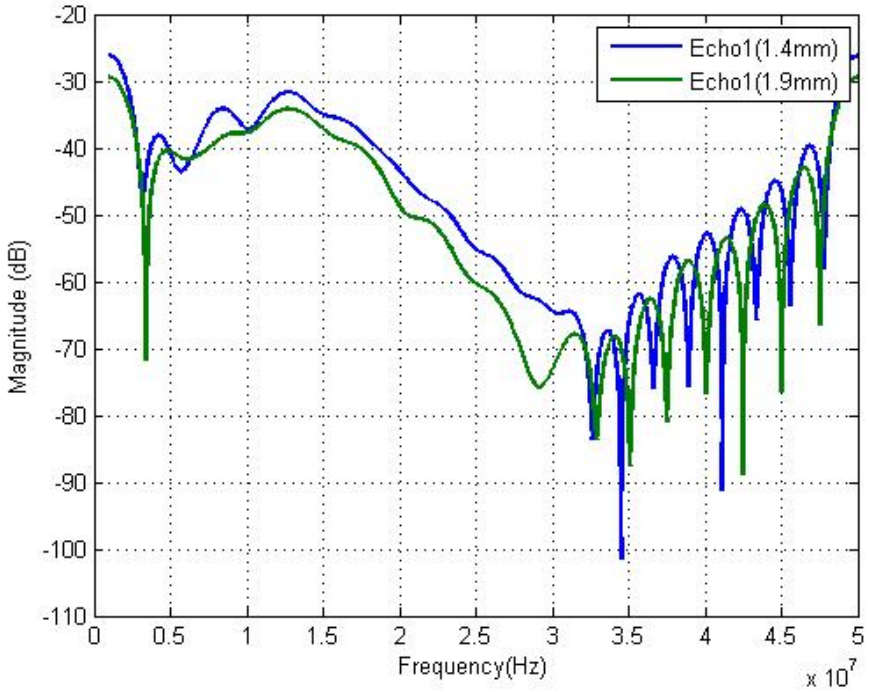

Figure 5.8: Combined plot of frequency response for the first echo at both 1.4mm and 1.9mm. CMUT without backing layer (from [8])

force applied to the CMUT since it did not have any room to move, being glued to the PCB, during the curing process.
This is the most likely scenario to affect the CMUT as observed, as this applied force can cause an increase in tension on the membrane. Increased membrane tension means increased spring constant, which leads to a shift in frequency to a higher level according to equation (2.23).

5.3 Impedance network

By finding the impedance response of the system, characteristic electrical properties can be identified. The network analyzer can not find the impedance response directly, but it can measure the real and imaginary parts of the reflection coefficient for the system. The impedance can be found by using the reflection coefficient, and a derivative of equation (2.29) which gives

$$Z = Z_0 \frac{1+\Gamma}{1-\Gamma}. \tag{5.5}$$

The resulting impedance response for the system is shown in Fig 5.9 and Fig 5.10. To find this response the HP8753E network analyzer had to be used. This was because the Rhode & Schwarts for unknown reasons gave different number of datapoints for the real and imaginary parts of the reflection coefficient. This resulted in trouble with the impedance calculations giving negative values of the real part, which can only be true for active components.

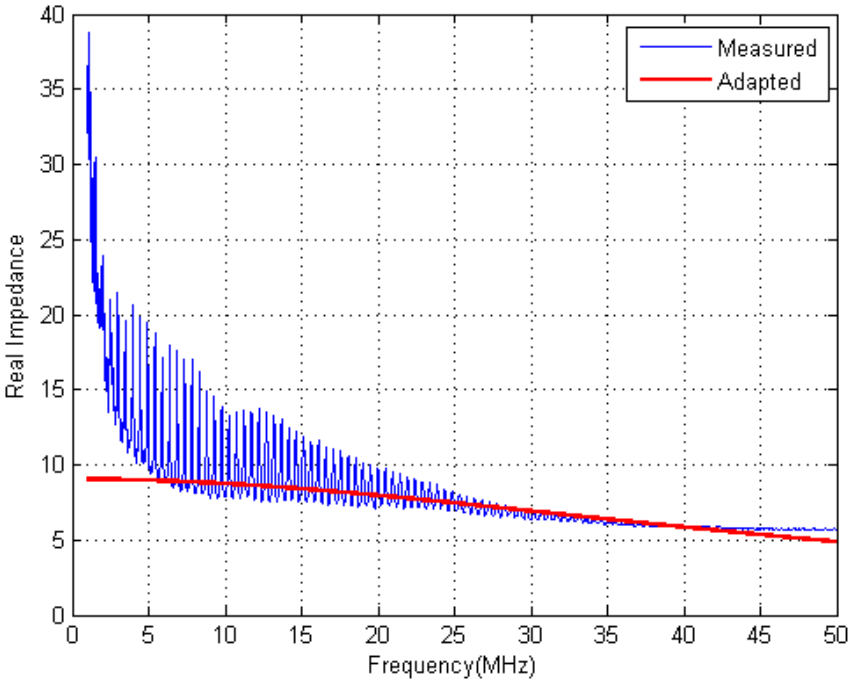

Figure 5.9: Real part of the impedance response of the system, with adapted curve.

By finding an impedance network with components comparable to the system, and with behaviour as close to the measured response as possible, a measure of the electrical properties of the system can be obtained. The network chosen for this case is shown in Fig 5.11.

The network analyzer is represented as a voltage source and 50Ω source impedance (R0). The capacitance C1 represents parasitic capacitance in the system, R1 represents line resistances, and C2 represents the CMUT.

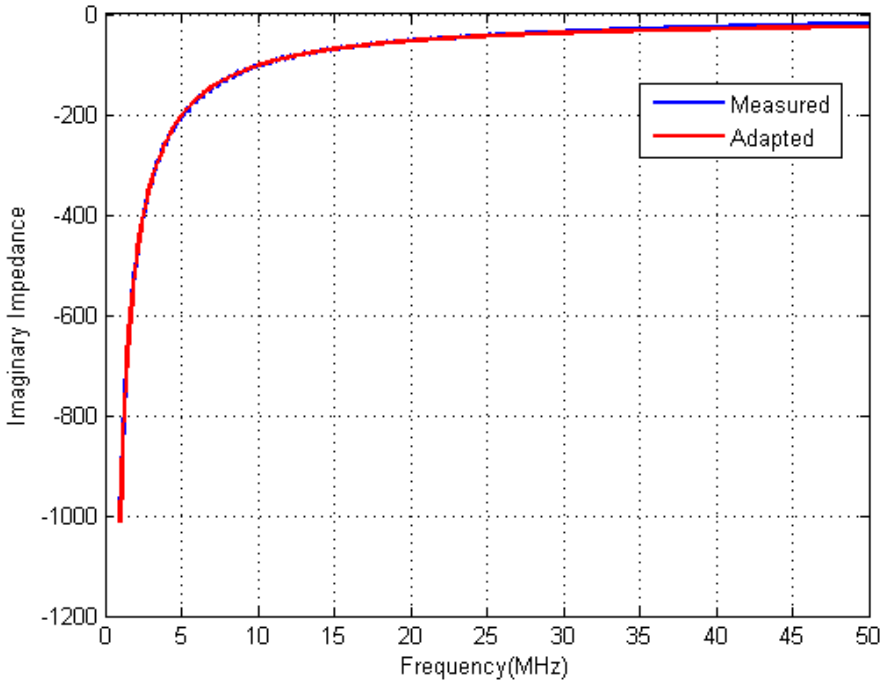

Figure 5.10: Imaginary part of the impedance response of the system, with adapted curve.

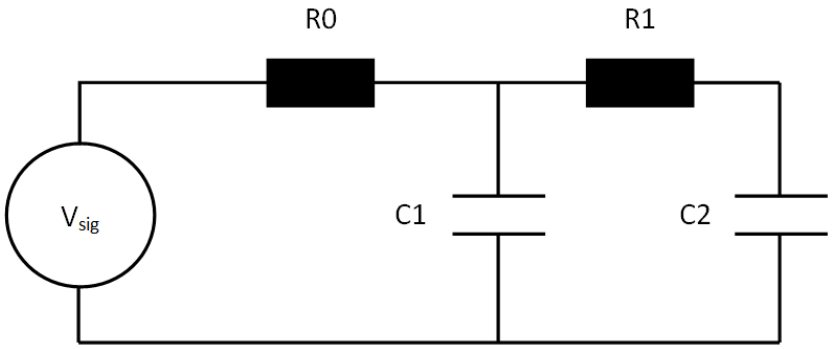

Figure 5.11: Impedance network for matching with the impedance response of the system.

The curves shown in Fig 5.9 and Fig 5.10 were considered to be the best adaption to the impedance responses. These were obtained with the following values

$$C1 = -j1500\Omega, \tag{5.6}$$
$$C2 = -j3100\Omega, \tag{5.7}$$
$$R1 = 85\Omega. \tag{5.8}$$

The adapted curve for the real part of the impedance response does not follow the measured values at lower frequencies. A better fit is however not possible with this impedance network. It is however considered to be good enough because parasitic disturbances from line capacitance, connections etc. at these lower frequencies can become quite dominant.

The impedance network shows quite high values of line resistance, and parasitic capacitances. This supports the theory from [8], that line resistance and parasitic capacitances causes disturbances in the CMUTs operation. The network also shows that there is a mismatch between the source and the load impedance. This could also be a contributor to the flat and unexpected frequency response the CMUT shows.

6. Conclusion and further work

The objective of this thesis was to continue the work to characterize a CMUT, started in [8]. The work in [8] was inconclusive, so a more thorough evaluation was desired. For this evaluation a backing layer was added to the CMUT. The hope was that this layer would have an effect on the CMUT that would give more stable responses to analyze. This effort proved however to be futile in terms of a more stable response, as apparently more instability arise in the responses. Gathering of precise values of center frequency and bandwidth of the CMUT has therefore been unsuccessful. The shape of the frequency response does however suggest that it has a wide bandwidth, and this is also supported by the short impulse responses.

A value for the attenuation of the rapeseed oil was found from measurements. It matched good with results presented in other articles, and the combined plot of echoes from $1.4mm$ and $1.9mm$ validated it with good matching of the responses.

Although characterization of the CMUT was partly unsuccessful, the measurements did provide insight on the performance of the backing material as an acoustic dampener, and effects the addition of a backing layer might have on a CMUT.
Comparing the impulse responses, with and without the backing layer, shows that the ringing is removed by the backing layer. The dimps that were present in the frequency response, has also been removed with the added backing. This confirms that the epoxy tungsten mixture has an acoustic impedance very similar to that of silicon, or reflections would occur in the silicon/backing layer interface which would allow the ringing to continue. The absorption factor of the backing layer seems to be good too, as there were no reflections from the free side of the layer. The thickness of the layer was however quite large, so commenting on its effectiveness for applications where a comparable layer cannot be achieved is not possible.

Another observation in the frequency response was that there was a significant increase in the response from about 20MHz ut to about 30MHz. This tendency was also present in the time gated frequency responses of the echoes. This increase is possibly due to a shift in the resonance frequency of the device, which means that there would have been alterations to the CMUT membrane. The most likely source of this is that the added backing layer changed in volume during curing, and by this putting a force on the CMUT. This may have caused an increase in the tension in the membrane, and thereby increasing its resonance frequency.

Lastly an impedance network adapted to the behaviour of the system, shows a presence of line resistance and parasitic capacitance that supports the theory from [8], that these deviations causes the device to function poorly and appear due to poor bonding and narrow lines on the CMUT. It also shows a mismatch with the source, which means that the power delivery to the CMUT might be quite poor for a range of frequencies.

Two rounds of testing without reaching the objective of characterizing the CMUT speaks in favor of finding a different CMUT to work on in future pulse-echo tests.
The shift in frequency that may be because of the backing layer exerting force on the CMUT, might be a topic for further study. It could at least be an idea to keep it in mind when adding backing in a confined space, as the hole in the PCB was in this case.

Bibliography

[1] C. J. L. Murray and A. Lopez, "Global mortality, disability, and the contribution of risk factors: Global burden of disease study," *The Lancet*, vol. 349, no. 9063, pp. 1436–1442, 1997.

[2] P.Libby, "Atherosclerosis: The new view," *Scientific American*, 2002.

[3] R. Seeley, *Essentials of Anatomy and Physiology*. Boston: McGraw Hill Higher Education, 2006.

[4] S. Glagov, E. Weisenberg, C. Zarins, R. Stankunavicius, and G. Kolettis, "Compensatory enlargement of human atherosclerotic coronary arteries," *The New England Journal of Medicine*, vol. 316, pp. 1371 – 1375, 1987.

[5] C. Zarins, E. Weisenberg, G. Kolettis, R. Stankunavicius, and S. Glagov, "Differential enlargement of artery segments in response to enlarging atherosclerotic plaques," *Journal of Vascular Surgery*, vol. 7, no. 3, pp. 386 – 394, 1988.

[6] T. Ytterdal, W. Booij, A. Dyrseth, H. Engan, T. Fjeldly, D. Hjelme, K. Ingebrigtsen, T. Njølstad, A. Rønnekleiv, T. Sæther, and D. Wang, "Smart microsystems in diagnostic imaging in medicine." *Application to the Research Counsil of Norway*.

[7] O. Oralkan, S. Hansen, B. Bayram, G. Yaralioglu, A. Ergun, and B. Khuri-Yakub, "High-frequency cmut arrays for high-resolution medical imaging," in *Ultrasonics Symposium, 2004 IEEE*, vol. 1, pp. 399–402 Vol.1, Aug. 2004.

[8] P. M. Ødelund, "Characterization of capacitive micromachined ultrasonic transducers," 2010.

[9] I. Ladabaum, P. Wagner, C. Zanelli, J. Mould, P. Reynolds, and G. Wojcik, "Silicon substrate ringing in microfabricated ultrasonic transduc-

ers," vol. 1, pp. 943 –946 vol.1, oct. 2000.

[10] C. Liu, *Foundations of Mems*. Upper Saddle River: Pearson Prentice Hall, 2006.

[11] I. Ladabaum, X. Jin, H. T. Soh, A. Atalar, and B. T. Khuri-Yakub, "Surface micromachined capacitive ultrasonic transducer," *IEEE Transactions on Ultrasonics, Ferroelectrics and Frequency Control*, vol. 45, no. 3, pp. 678–690, 1998.

[12] A. S. Ergun, G. G. Yaralioglu, and B. T. Khuri-Yakub, "Capacitive micromachined ultrasonic transducers: Theory and technology," *Journal of Aerospace Engineering*, vol. 16, no. 2, pp. 76–84, 2003.

[13] H. Martinussen, *Heterodyne interferometry for dynamic and static characterization of micro- and nanostructures*. PhD thesis, 2009.

[14] D. Raichel, *The Science and Applications of Acoustics*. Fort Collins: Springer Science+business Media, 2006.

[15] S. Kocis, *Ultrasonic Measurements and Technologies*. London: Chapman & Hall, 1996.

[16] F. Pedrotti, *Introduction to Optics*. Upper Saddle River: Pearson Education, 2006.

[17] W. Hedrick, *Ultrasound Physics and Instrumentation*. St.Louis: Elsevier Mosby, 2005.

[18] J. Marini and J. Rivenez, "Acoustical fields from rectangular ultrasonic transducers for non-destructive testing and medical diagnosis," *Ultrasonics*, vol. 12, no. 6, pp. 251 – 256, 1974.

[19] B. Bayram, E. Haeggstrom, G. Yaralioglu, and B. Khuri-Yakub, "A new regime for operating capacitive micromachined ultrasonic transducers," *IEEE Transactions on Ultrasonics, Ferroelectrics and Frequency Control*, vol. 50, pp. 1184–1190, Sept. 2003.

[20] S. Martini, C. Bertoli, M. L. Herrera, I. Neeson, and A. Marangoni, "Attenuation of ultrasonic waves: Influence of microstrucktures and solid fat content," *Journal of the American Oil Chemists' Society*, vol. 82, no. 5, pp. 319 – 328, 2005.

[21] A. Ronnekleiv, K. Midtbo, and D. T. Wang, "5i-5 fabrication and characterization of cmuts realized by wafer bonding," in *Ultrasonics Symposium, 2006. IEEE*, pp. 938–941, Oct. 2006.

[22] J. N. Coupland and D. J. McClements, "Physical properties of liquid edible oils," *JAOCS, Journal of the American Oil Chemists' Society*, vol. 74, no. 12, pp. 1559–1564, 1997.

[23] "Olympus panametrics-ndt: Ultrasonic transducers technical notes," p. 46.

[24] R. Chanamai and D. J. McClements, "Ultrasonic attenuation of edible oils," *JAOCS, Journal of the American Oil Chemists' Society*, vol. 75, no. 10, pp. 1447–1448, 1998.

[25] A. Logan and J. Yeow, "Fabricating capacitive micromachined ultrasonic transducers with a novel silicon-nitride-based wafer bonding process," *Ultrasonics, Ferroelectrics and Frequency Control, IEEE Transactions on*, vol. 56, pp. 1074 –1084, may 2009.

[26] H. Wang, T. Ritter, W. Cao, and K. Shung, "High frequency properties of passive materials for ultrasonic transducers," *IEEE Transactions on Ultrasonics, Ferroelectrics and Frequency Control*, vol. 48, no. 1, pp. 78 – 84, 2001.

[27] R. Webster, T. Button, C. Meggs, D. MacLennan, and S. Cochran, "P3k-5 passive materials for high frequency ultrasound components," in *Ultrasonics Symposium, 2007. IEEE*, pp. 1925 –1928, 28-31 2007.

Appendices

A. Olympus Panametrics-NDT transducer characteristics

OLYMPUS

Tel: 781-419-3900
www.olympusndt.com

TRANSDUCER DESCRIPTION

PART NO.: V310
SERIAL NO.: 601326
DESIGNATION: IMMERSION

FREQUENCY: 5.00 MHz
ELEMENT SIZE: .25 IN. DIA.

TEST INSTRUMENTATION

PULSER/RECEIVER: PANAMETRICS 5052UA #1
DIGITAL OSCILLOSCOPE: LeCroy LT342 / SN: LT34202249
TEST PROGRAM: TP103-3 VER. 10814H
CABLE: RG-58 A/U LENGTH: 4FT

TEST CONDITIONS

PULSER SETTING: ENERGY: 4 ; DAMPING: 50 OHM
RECEIVER SETTING: ATTN: 44dB ; GAIN: 40dB
TARGET: 2 in. SILICA
JOB CODE: TP200

WATER PATH: 1.012 in

MEASUREMENTS PER ASTM E1065

WAVEFORM DURATION:
-14DB LEVEL --- 0.344 US
-20DB LEVEL --- 0.368 US
-40DB LEVEL --- 0.712 US

SPECTRUM MEASURANDS:
CENTER FREQ. ------ 4.94 MHz
PEAK FREQUENCY -- 4.6 MHz
-6DB BANDWIDTH --- 77.76 %

COMMENTS:

F#: 4.94

** ACCEPTED

TECHNICIAN (3) David Santiago

DATE: 10-05-2007

SIGNAL WAVEFORM

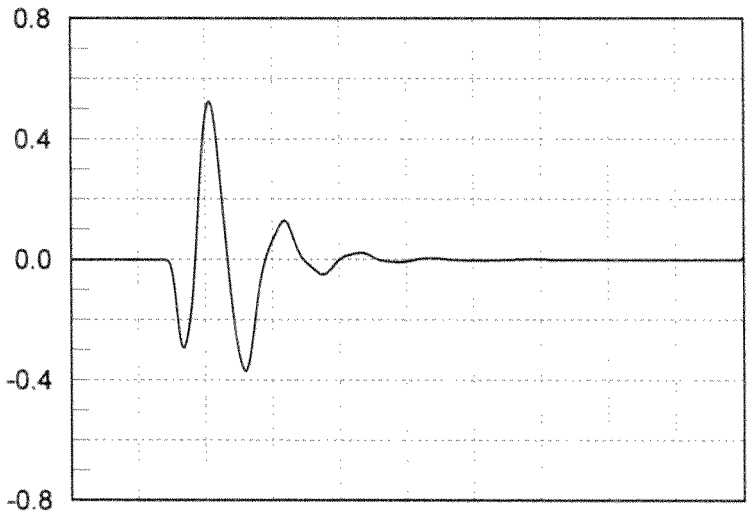

(.2 USEC / DIVISION)

FREQUENCY SPECTRUM

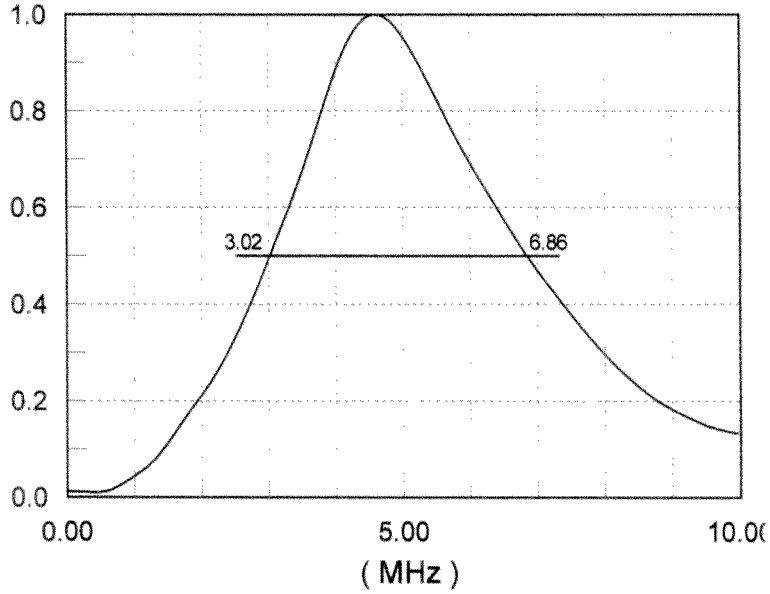

(MHz)

PANAMETRICS-NDT

OLYMPUS

Tel: 781-419-3900
www.olympusndt.com

TRANSDUCER DESCRIPTION

PART NO.: V312
SERIAL NO.: 616419
DESIGNATION: IMMERSION

FREQUENCY: 10.00 MHz
ELEMENT SIZE: .25 in. DIA.

TEST INSTRUMENTATION

PULSER/RECEIVER: PANAMETRICS 5052UA #1
DIGITAL OSCILLOSCOPE: LeCroy LT342 / SN: LT34202249
TEST PROGRAM: TP103-3 VER. 10814H
CABLE: RG 174/U LENGTH: 4FT

TEST CONDITIONS

PULSER SETTING: ENERGY: 1 ; DAMPING: 50 OHMS
RECEIVER SETTING: ATTN: 42dB ; GAIN: 40dB
TARGET: 2 IN SILICA
JOB CODE: TP200

WATER PATH: .995 in

MEASUREMENTS PER ASTM E1065

WAVEFORM DURATION:
-14DB LEVEL --- 0.142 US
-20DB LEVEL --- 0.196 US
-40DB LEVEL --- 0.418 US

SPECTRUM MEASURANDS:
CENTER FREQ. ------ 10.97 MHz
PEAK FREQUENCY -- 11.92 MHz
-6DB BANDWIDTH --- 96.77 %

COMMENTS:

F#: 10.96

SIGNAL WAVEFORM

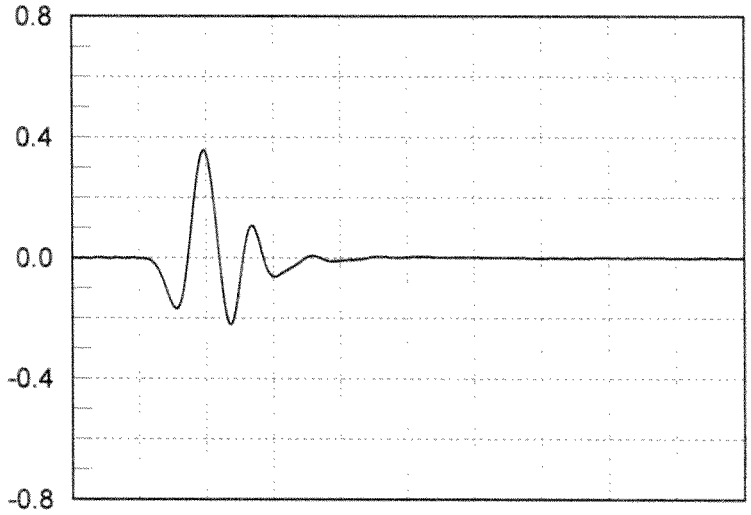

(.1 USEC / DIVISION)

FREQUENCY SPECTRUM

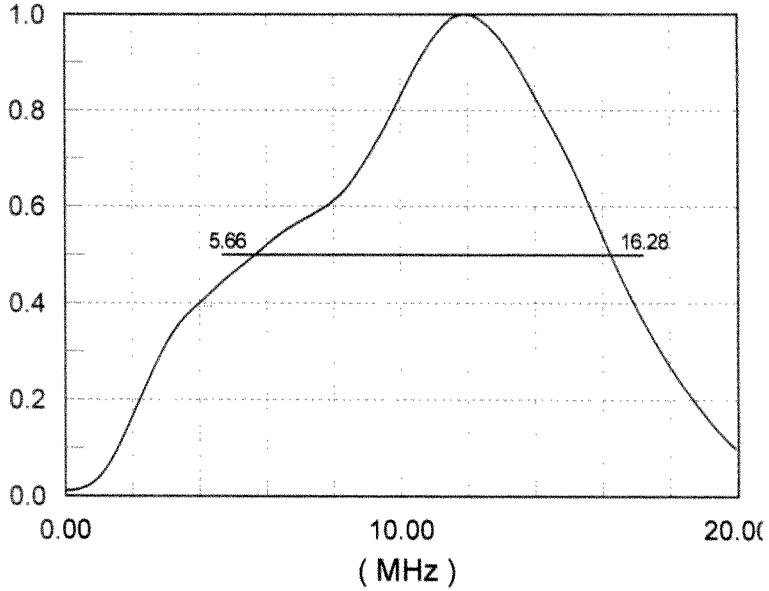

(MHz)

** ACCEPTED

TECHNICIAN (3) David Santago

DATE: 02-28-2008

PANAMETRICS-NDT

OLYMPUS

Tel: 781-419-3900
www.olympusndt.com

TRANSDUCER DESCRIPTION

PART NO.: V313
SERIAL NO.: 632653
DESIGNATION: IMMERSION

FREQUENCY: 15.00 MHz
ELEMENT SIZE: .25 in. DIA.

TEST INSTRUMENTATION

PULSER/RECEIVER: PANAMETRICS 5052UA #6
DIGITAL OSCILLOSCOPE: LeCroy LC564A / SN: LC56410253
TEST PROGRAM: TP103-3 VER. 1084TA
CABLE: RG-58 A/U LENGTH: 4FT

TEST CONDITIONS

PULSER SETTING: ENERGY: 1 ; DAMPING: 50
RECEIVER SETTING: ATTN: 40dB ; GAIN: 40dB
TARGET: 2 in. SILICA
JOB CODE: TP200

WATER PATH: .979 in

MEASUREMENTS PER ASTM E1065

WAVEFORM DURATION:
-14DB LEVEL --- 0.146 US
-20DB LEVEL --- 0.156 US
-40DB LEVEL --- 0.318 US

SPECTRUM MEASURANDS:
CENTER FREQ. ------ 14.7 MHz
PEAK FREQUENCY -- 15.3 MHz
-6DB BANDWIDTH --- 72.43 %

COMMENTS:

F#: 14.67

** ACCEPTED

TECHNICIAN (7)

DATE: 05-19-2008

SIGNAL WAVEFORM

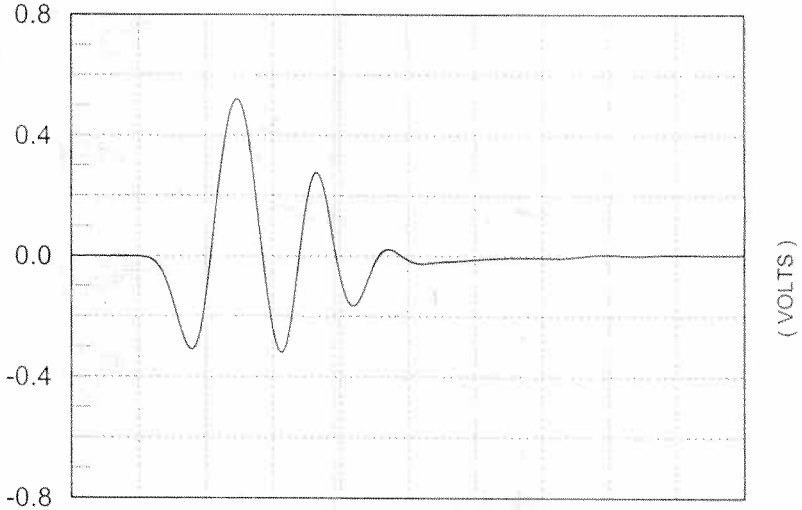

(.05 USEC / DIVISION)

FREQUENCY SPECTRUM

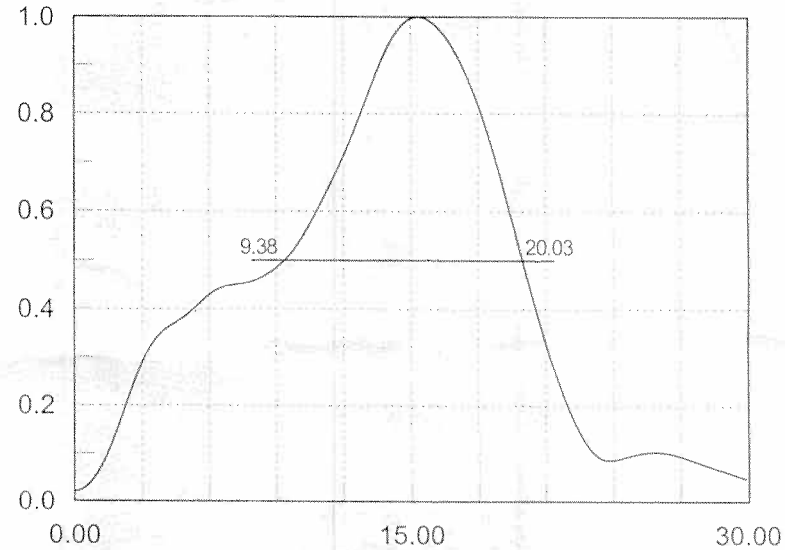

PANAMETRICS-NDT

TP1XX Rev. A TEG Drwg# 16150

OLYMPUS

Tel: 781-419-3900
www.olympusndt.com

TRANSDUCER DESCRIPTION

PART NO.: V317
SERIAL NO.: 625453
DESIGNATION: IMMERSION

FREQUENCY: 20.00 MHz
ELEMENT SIZE: .25 in. DIA.

TEST INSTRUMENTATION

PULSER/RECEIVER: PANAMETRICS 5052UA #6
DIGITAL OSCILLOSCOPE: LeCroy LC564A / SN: LC56410253
TEST PROGRAM: TP103-3 VER. 10814H
CABLE: RG-58A/U LENGTH: 4FT.

TEST CONDITIONS

PULSER SETTING: ENERGY: 1 ; DAMPING: 50
RECEIVER SETTING: ATTN: 34dB ; GAIN: 40dB
TARGET: 2 in. SILICA
JOB CODE: TP200

WATER PATH: 1.031 in

MEASUREMENTS PER ASTM E1065

WAVEFORM DURATION:
-14DB LEVEL --- 0.138 US
-20DB LEVEL --- 0.162 US
-40DB LEVEL --- 0.302 US

SPECTRUM MEASURANDS:
CENTER FREQ. ------ 19.41 MHz
PEAK FREQUENCY -- 19.76 MHz
-6DB BANDWIDTH --- 48.18 %

COMMENTS:

F#: 19.4

** ACCEPTED

TECHNICIAN (7)

DATE: 03-26-2008

SIGNAL WAVEFORM

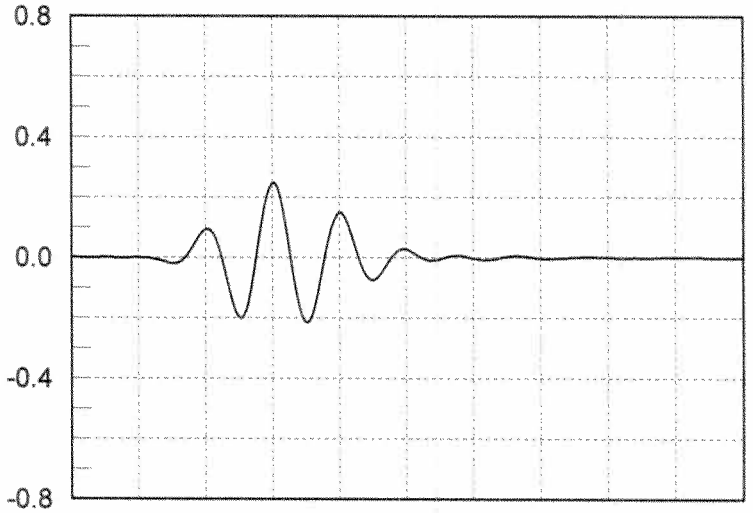

(.05 USEC / DIVISION)

FREQUENCY SPECTRUM

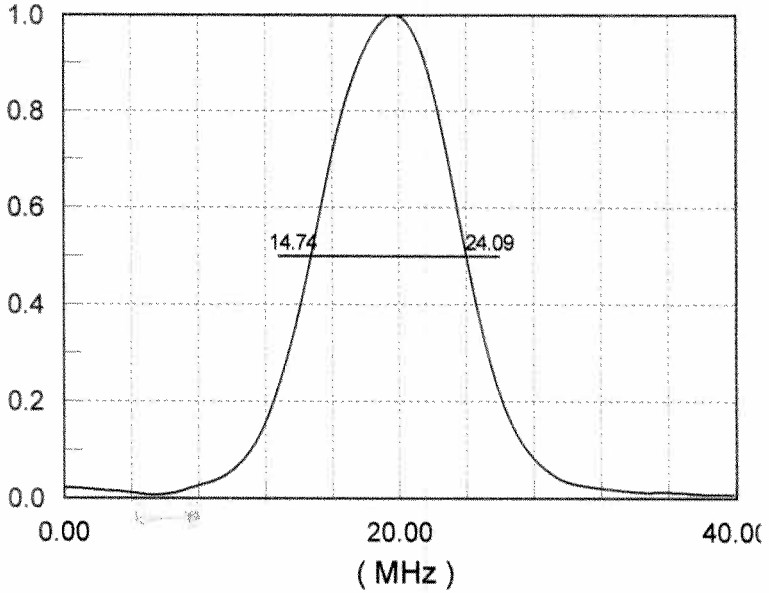

PANAMETRICS-NDT